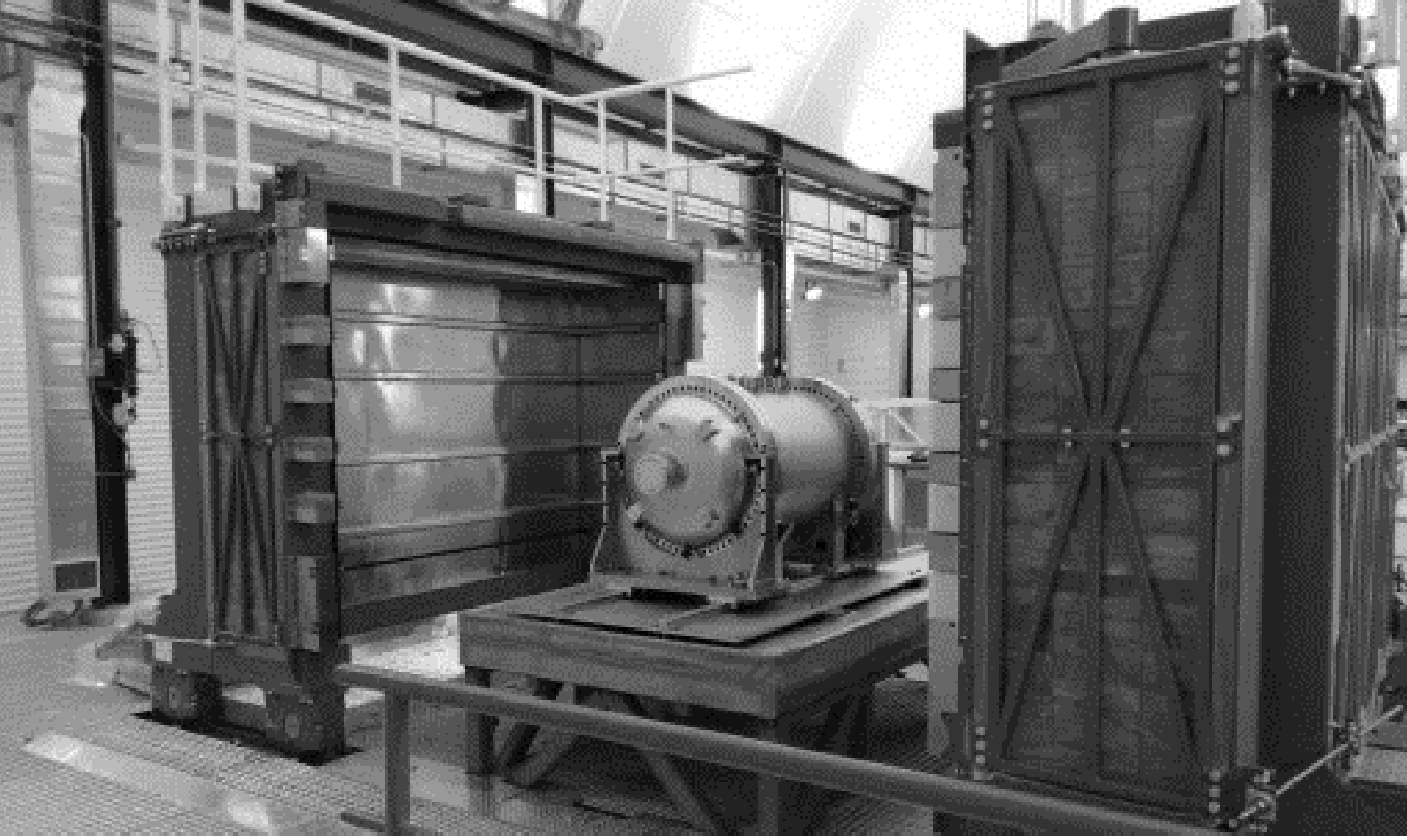

Rui Daniel Passos Mano

Experimental Measurement of the Electroluminescence Yield, Electron Drift Velocity and Intrinsic Energy Resolution for Mixtures of Xenon with sub-percentage quantities of CO_2 for the NEXT Experiment

Tese de mestrado em Mestrado em Física

Setembro de 2015

· U C ·

UNIVERSIDADE DE COIMBRA

Rui Daniel Passos Mano

Experimental Measurement of the Electroluminescence Yield, Electron Drift Velocity and Intrinsic Energy Resolution for Mixtures of Xenon with sub-percentage quantities of CO_2 for the NEXT Experiment

Dissertation submitted to Faculdade de Ciências e Tecnologia da Universidade de Coimbra for the Master's degree in Physics, under the supervision of Dr. Cristina Maria Bernardes Monteiro and of Dr. Elisabete Dinora Caldas de Freitas.

2015

UNIVERSIDADE DE COIMBRA

Acknowledgements

À Doutora Cristina Monteiro, pela orientação neste trabalho experimental, por todas as dúvidas esclarecidas e pela ajuda que deu na escrita desta dissertação.

À Doutora Elisabete Freitas, pela orientação neste trabalho experimental e pela disponibilidade que sempre demonstrou nos momentos em que precisei de ajuda.

Ao Professor Doutor Joaquim Marques Ferreira dos Santos, por me ter dado a oportunidade de trabalhar neste excelente grupo de investigação onde fui tão bem recebido e onde aprendi tanto. Agradeço também por todos os comentários sábios que deu acerca deste trabalho.

Ao Doutor Luís Fernandes, por toda a ajuda que nos deu quando tivemos problemas com o sistema experimental.

Ao Doutor Fernando Amaro, por todos os conselhos que foi dando ao longo do tempo acerca da escrita da dissertação.

Ao Xavier e ao Emanuel por toda a amizade e por sempre me acompanharem desde o início do meu percurso académico.

Ao Carlos Henriques, ao Pedro Borlido, e à Marina Jorge pela amizade e pela paciência que sempre tiveram para me tirar qualquer dúvida que tivesse.

Ao Hugo e ao Filipe pela amizade desde sempre.

Aos meus pais, o maior agradecimento, por todo o apoio que me deram e pelos sacrifícios que fizeram para que eu conseguisse este objetivo.

Abstract

The nature of neutrinos is one of the most important questions in the physical world. Its answer would have a great impact in many fields such as particle physics, cosmology and experimental neutrino physics. This nature can be tested through the detection of the double beta decay process without the emission of neutrinos. If a positive signal for neutrinoless double beta decay is confirmed there will be no doubt that the neutrinos are Majorana particles, instead of Dirac particles, as was postulated in the Standard Model of Particle Physics.

The NEXT collaboration is developing a HPXeTPC that uses an electroluminescence process as amplification of the primary ionization signal resulting from radiation interactions in the sensitive volume. The Electroluminescence process allows an effective signal amplification with reduced statistical fluctuations when compared to the signal amplification through the charge avalanche processes. A very good energy resolution is mandatory for an efficient discrimination of the Xe neutrinoless double beta decay events from the background not only due to gamma-interactions but also due to the double beta decay events with the emission of neutrinos, a mechanism that is several order of magnitude more frequent than the $\beta\beta0\nu$.

The capability of pattern recognition of the $\beta\beta0\nu$ primary ionization track, will allow a further discrimination of the $\beta\beta$ events from those resulting from gamma interactions. However, Xe is a slow gas with a large electron diffusion, factors that present a drawback for such discrimination. The addition of molecular additives to pure xenon will have a significant impact in the reduction of the primary electron cloud diffusion and in the increase of the electron drift velocity in the mixture. However, such additives will also lead to a reduction of the mixture scintillation Yield and an increase of the statistical fluctuations associated with the electroluminescence production, since a collision between a drifting electron and a molecule may absorb the electron kinetic energy to vibrational and rotational states, without leading to electroluminescence. A compromise between the concentration of the molecular additive and the reduction of the electroluminescence yield or the increase of the statistical fluctuations associated the EL production is needed to be investigated.

Resumo

A natureza dos neutrinos é uma das questões mais importantes na atualidade da física. A sua resposta terá um grande impacto em diferentes campos da física, como por exemplo na física de partículas, na cosmologia e na física experimental de neutrinos. Esta natureza pode ser testada através da deteção do processo de decaimento beta duplo sem emissão de neutrinos. Se este decaimento se confirmar não haverá dúvida de que os neutrinos são partículas de Majorana, em vez de partículas de Dirac, como o Modelo Padrão da Física de Partículas assume.

A experiência NEXT está a desenvolver uma TPC com xénon a alta pressão e que usa o processo de eletroluminescência como meio de amplificação do sinal de ionização primária, causada pelas interações da radiação com o meio gasoso. O processo de eletroluminescência permite uma amplificação de sinal efetiva com reduzidas flutuações estatísticas quando comparadas com o processo de amplificação de sinal através de multiplicação em carga. É necessário atingir uma resolução em energia muito boa para obter uma discriminação eficiente do decaimento beta duplo sem emissão de neutrinos no xénon, tanto do fundo provocado pelas interações gama, como do próprio decaimento beta duplo com emissão de neutrinos. Este último é um mecanismo algumas ordens de grandeza mais frequente do que o $\beta\beta0\nu$.

A capacidade de reconhecimento da topologia da ionização primária do evento $\beta\beta0\nu$ possibilitará uma posterior distinção dos eventos $\beta\beta$ dos eventos resultantes das interações gama. No entanto, o xénon é um gás muito lento com elevada difusão de eletrões, sendo estes fatores uma desvantagem para a distinção acima referida. A adição de aditivos moleculares ao xénon puro terá um impacto significativo na redução da difusão da nuvem de eletrões primária e no aumento da velocidade de deriva dos eletrões na mistura. Contudo, estes aditivos causarão também uma redução do rendimento de cintilação da mistura e um aumento das flutuações estatísticas associadas à produção de eletroluminescência uma vez que o eletrão de deriva, ao colidir com uma molécula, irá perder parte da sua energia cinética para os estados vibracionais e rotacionais desta, não havendo desta forma produção de cintilação.

Portanto, terá de ser feito um compromisso entre a concentração de aditivo molecular e a redução do rendimento de eletroluminescência ou o aumento das flutuações estatísticas associadas à produção de eletroluminescência, sendo este o estudo efetuado neste trabalho.

List of Figures

List of Tables

List of Abbreviations

SM – Standard Model

TPC - Time Projection Chamber

NEXT – Neutrino Experiment with a Xenon TPC

HPXe – High Pressure Xenon

GIAN – Atomic and Nuclear Instrumentation Group

MC – Monte Carlo

EL – Electroluminescence

GPSC – Gas Proportional Scintillation Counter

ββ – Double beta decay

Z – Atomic number

A – Mass number

ββ2ν – Standard double beta decay

ββ0ν - Neutrinoless double beta decay

HM - Heidelberg-Moscow

IGEX - International Germanium Experiment

LNGS - Laboratori Nazionali del Gran Sasso

HPGe – High Purity Germanium

NEMO - Neutrino Ettore Majorana Observatory

GERDA - GERmanium Detector Array

CUORE - Cryogenic Underground Observatory for Rare Event

LXeTPC – Liquid Xenon TPC

EXO - Enriched Xenon Observatory

LSC – Laboratorio Subterráneo de Canfranc

IFIC – Instituto de Física Corpuscular

PMT – Photomultiplier Tube

SiPM – Silicon Photomultiplier

SOFT – Separated Optimized Functions for Tracking

VUV – Vacuum Ultraviolet

PC – Proportional Counter

APD – Avalanche Photodiode

FWHM – Full width at half maximum

WIMPs – Weak Interactive Massive Particles

Table of Contents

1. Introduction

1.1. Neutrinos

Neutrinos are the second most abundant particles in the universe next to photons.

The standard model (SM) of particle physics describes neutrinos as massless and neutral elementary particles of spin ½. Consequently, they would only interact through the weak force being very difficult to detect.

Neutrinos are leptons and have three different flavors, one for each of the three charged leptons, e (electron), μ (muon) and τ (tau). Lepton number is conserved separately for each of the three lepton families (e, ν_e), (μ, ν_μ), (τ, ν_τ) and this rule cannot be violated.

All neutrinos are left-handed and all antineutrinos are right-handed, and since they are massless this handedness cannot be altered.

They were first postulated by Wolfgang Pauli in 1930 in order to explain the continuum energy spectrum of beta particles emitted in the single beta decay. In 1995, Clyde Cowan and Fred Reines experimentally discovered the electron neutrino [1], and this discovery granted Reines the Nobel Prize in 1995 (Cowan had already passed away at the time).

The SM was developed in the 70's and since then it has been a very successful theory, providing an excellent description of most of the particle physics phenomena. However, its description of neutrinos has not stood up to the experimental evidences and the SM had to be modified in this sector. The main boosters of these modifications were the so called Solar Neutrino Problem [2] and the Atmospheric Neutrino Anomaly [3].

In 1957, the Italian physicist Bruno Pontecorvo proposed that neutrinos oscillated in flavor when they travelled astronomical distances and this quantum mechanical phenomenon was denominated of neutrino oscillation [4]. These neutrino oscillations arise from the mixture between the flavor and mass eigenstates of neutrinos. A neutrino created with a flavor α could be detected afterwards in a distinct flavor state β with a certain probability, after traveling a distance z. This is due to the fact that there are small differences in the masses of its mass eigenstates.

A flavor state can be described mathematically as a combination of the three mass eigenstates:

$$|\nu_\alpha\rangle = \sum_i U^*_{\alpha i} |\nu_i\rangle \quad (1)$$

where $|\nu_\alpha\rangle$ is a neutrino in a flavor state α = e, μ or τ, $|\nu_i\rangle$ is a neutrino in a mass state m_i, i = 1, 2 or 3 and $U_{\alpha i}$ are elements of the neutrino mixing matrix [4].

This proposal was in fact the solution to the discrepancy observed in the measurements of solar and atmospheric neutrinos. The proof of Neutrino Oscillation implied that neutrinos had mass in contrast to the SM prediction.

In 1937 Ettore Majorana formulated a theory of neutrinos in which the neutrino and antineutrino were the same particle, being the neutrino a Majorana particle [5]. This Majorana nature of the neutrino could be experimentally tested through detection of a Double Beta Decay ($\beta\beta$) process without emission of neutrinos.

1.2. Double Beta Decay

Double beta decay is a very slow process that converts an initial nucleus of atomic number Z and mass number A, (Z, A), into a nucleus of (Z-2, A) or (Z +2, A), considering the two possible modes $\beta^+\beta^+$ and $\beta^-\beta^-$, respectively. In the following text, only the $\beta^-\beta^-$ process will be discussed and it will be simply denoted as $\beta\beta$.

There are two different modes of $\beta\beta$, the Standard Double Beta Decay ($\beta\beta2\nu$) and the Neutrinoless Double Beta Decay ($\beta\beta0\nu$).

1.2.1 Standard Double Beta Decay

Standard double beta decay was proposed in 1935 by Maria Goeppert-Mayer [6]. ββ2ν is the process of the simultaneous beta decay of two neutrons in a nucleus.

$$(Z, A) \rightarrow (Z + 2, A) + e_1^- + e_2^- + \bar{\nu}_{e_1} + \bar{\nu}_{e_2} \quad (2)$$

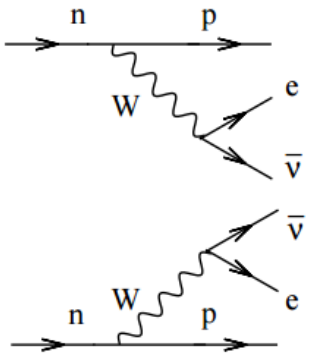

Figure 1.1. Feynman diagram for $\beta\beta 2\nu$ [7].

This decay conserves electric charge and lepton number, being this process allowed by the SM.

This process was observed for the first time in 1987 in ^{82}Se [8]. In the meantime, it has been observed in many other nuclei, with half lives in the range of 10^{18} to 10^{24} years [9].

This process can only occur if the single beta decay mode is not possible (Figure 1.2).

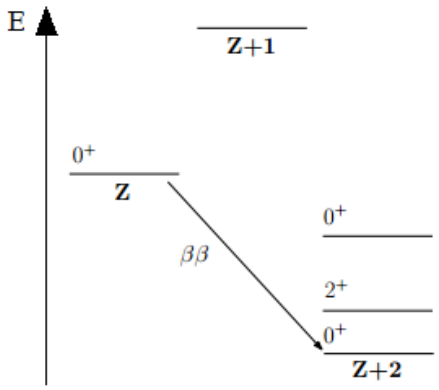

Figure 1.2. Generic level diagram of a $\beta\beta$ decay (modified from [8])

1.2.2. Neutrinoless Double Beta Decay

Neutrinoless double beta decay was proposed in 1937 by Giulio Racah as a way to test the Majorana nature of the neutrino [10], and in 1939 Wendell H. Furry calculated the approximate rates for ββ0ν [11].

This process is only possible if neutrinos have mass and if they are its own antiparticle.

In this decay, two neutrons in a nucleus decay simultaneously into two protons, with the emission of two electrons. However, in this case there is no emission of neutrinos. Figure 1.3 shows the Feynman diagram for the ββ0ν process, where a neutron decays with the emission of a right-handed ν_e and is absorbed afterwards as a left-handed ν_e.

$$(Z, A) \rightarrow (Z + 2, A) + e_1^- + e_2^- \quad (3)$$

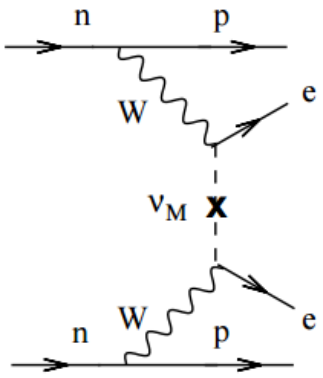

Figure 1.3. Feynman diagram for ββ0*ν* [7]

This decay is only possible if neutrinos are Majorana particles, that is, neutrinos and antineutrinos are indistinguishable and annihilate. All other SM fermions, being electrically charged, are instead Dirac particles, distinguishable from their own antiparticles.

Many mechanisms were proposed to describe ββ0ν. The simplest is the exchange of light Majorana neutrinos. Therefore, if this process is assumed to be the dominant one at low energies, the half-life of ββ0ν is written as:

$$\left(T_{1/2}^{0\nu}\right)^{-1} = G^{0\nu}\left|M^{\beta\beta0\nu}\right|^2 m_{\beta\beta}^2 \quad (4)$$

where $G^{0\nu}$ is an accurately calculated phase space integral, $M^{\beta\beta0\nu}$ is the nuclear matrix element of the transition, which has to be evaluated theoretically, and $m_{\beta\beta}$ is the effective Majorana mass of the electron neutrino:

$$m_{\beta\beta} = \left|\sum_i U_{\alpha i}^2 m_i\right| \quad (5)$$

where m_i are the neutrino mass eigenstates and $U_{\alpha i}^2$ are elements of the neutrino mixing matrix.

The discovery of this hypothetical process would prove the Majorana nature of the neutrino and, at the same time, would give direct information on its mass and why this mass should be so small when compared with the mass of all the other fermions.

Furthermore, the observation of ββ0ν will show that this process violates lepton number conservation. This result can be linked to the asymmetry between matter and antimatter in the Universe through the process known as leptogenesis [12]. For all of these reasons the discovery of ββ0ν would have a great impact in the physics world. Therefore, there are several experiments occurring around the world that are trying to measure this decay. However, to date, no convincing experimental evidence for this mode exists [13], although there was already a claim from the Heidelberg-Moscow experiment [14] in 2001.

1. 3. ββ0ν Experiments

ββ0ν experiments have in general two main objectives: measure the kinetic energy of the emitted electrons and measure the half-life time of the process.

In this decay, the sum of the kinetic energies of the emitted electrons is equal to the mass difference of the parent nucleus and the daughter nucleus, $Q_{\beta\beta}$, since there are no emitted neutrinos to share the energy with

$$Q_{\beta\beta} \equiv M(Z, A) - M(Z + 2, A) \tag{6}$$

In Figure 1.4 the spectrum of energy of the ββ2ν decay and the energy spectrum of the ββ0ν decay are plotted. Due to the finite energy resolution of any detector, the ββ0ν events are reconstructed in a certain range of energies, following a Gaussian distribution, centred on the Q value.

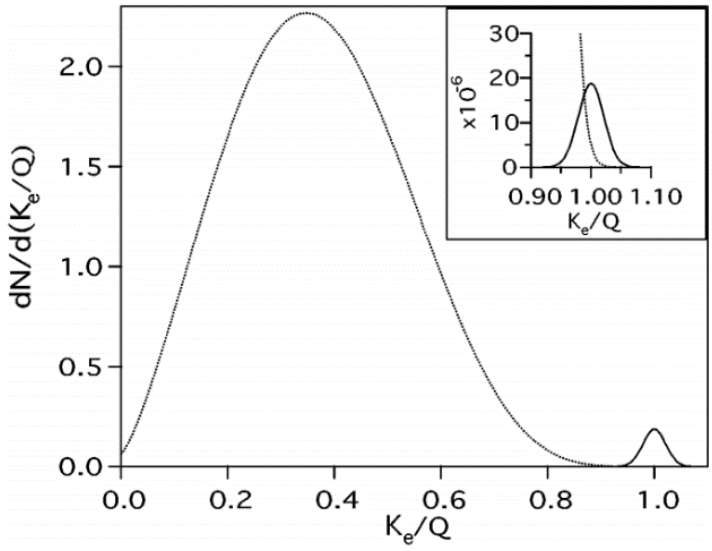

Figure 1.4. Double beta decay spectrum. The continuous part is the spectrum of the ββ2ν process while the peak to the right corresponds to the ββ0ν process [8].

Other processes can fall in these energy ranges, for example, the ββ2ν, which is an intrinsic background in all of these experiments and can only be distinguished if the detector has a good energy resolution. These backgrounds will compromise the sensitivity of the experiment and will "smear" the Q-value peak.

The measure of the half-life of the process is limited by the experimental sensitivity of the detector used and can be expressed as:

$$T_{1/2} \propto a.\epsilon.\sqrt{\frac{M.t}{\Delta E.B}} \quad (7)$$

where M is the mass of the isotope used, t is the time of active data acquisition of the detector, ΔE is the energy resolution in the region of interest, ϵ is the detection efficiency, a is a term which includes nuclear matrix elements and B is the background rate in the same region of interest.

1.3.1. State of art of ββ0υ experiments

There are several experiments that are searching for the ββ0υ using different techniques and different types of detectors with increasing sensitivities. These searches are carried out using *direc*t and *indirect methods*.

Indirect methods measure the concentration of daughter nuclei in a material after long time exposures. These are divided into radiochemical and geochemical experiments.

In a radiochemical experiment, the daughter nucleus has to be also radioactive and this method has been used in the study of ^{138}U [16].

A geochemical experiment searches for an excess of daughter nuclei in materials with a high concentration of ββ. This technique has been used to study ^{82}Se [17], ^{128}Te and ^{130}Te [18][19].

The *direct method* is currently the most used in these type of studies. The aim of this method is to measure the properties of the two electrons emitted in ββ decay. The detectors used can be *homogeneous*, if the source also acts as the detection medium, or they can be *inhomogeneous*, if an external source is introduced inside the detector.

Examples of past experiments that used homogeneous detectors are the Heidelberg-Moscow (HM) experiment [14], the International Germanium Experiment (IGEX) [20], both searching for ββ0ν in ^{76}Ge, and the CUORICINO experiment that used cryogenic TeO_2 bolometers [21].

The HM experiment ran from 1990 to 2003 in the Laboratori Nazionali del Gran Sasso (LNGS), Italy, and searched for $\beta\beta0\nu$ in ^{76}Ge using five p-type HPGe detectors [22]. In 2001, part of the Heidelberg collaboration claimed an observation of a $\beta\beta0\nu$ signal [14]. However, this results was not accepted by some members of the community and even by some members of the same collaboration [23][24]. The main goal of the future experiments is to search for $\beta\beta0\nu$ signals in the limits established by the HM experiment.

NEMO3 (Neutrino Ettore Majorana Observatory) is an example of an experiment where an inhomogeneous detector was used and its description can be found in [25].

Many present experiments are doing efforts to search for a positive $\beta\beta0\nu$ signal. The germanium calorimeters are used in experiments such as GERDA (GERmanium Detector Array) [26] and MAJORANA [27]. CUORE (Cryogenic Underground Observatory for Rare Event) [28] is an extension of CUORICINO using cryogenic TeO_2 bolometers. KamLand-Zen [29] and BOREXINO [30] experiments dissolve xenon gas in an organic scintillator.

EXO (Enriched Xenon Observatory) [31] uses a liquid xenon TPC (LXeTPC) to search for $\beta\beta0\nu$ in ^{136}Xe. The NEXT collaboration [13] is developing an experiment to do this search in the same isotope as EXO but using a HPXeTPC, as will be explored in section 1.4.

1.3.2. $\beta\beta0\nu$ Xenon Experiments

Xenon is an element with very interesting characteristics. It can act either as a source of $\beta\beta0\nu$ events as well as a detector for these events. It has two natural isotopes that can decay by $\beta\beta2\nu$, namely, the ^{134}Xe ($Q_{\beta\beta}$ = 825keV) and the ^{136}Xe ($Q_{\beta\beta}$ = 2458keV). The ^{136}Xe isotope is the obvious choice, since it has a higher $Q_{\beta\beta}$ value and the radioactive background is less prominent at higher energies. The $\beta\beta2\nu$ mode is slow, compared with other isotopes, and the process of isotopic enrichment is relatively simple and cheap.

1.3.3. Xenon TPCs for ββ0ν searches

A xenon TPC is a fully active detector in which xenon acts simultaneously as source and detector of ββ0ν. It combines all the advantages of the use of this noble gas with the possibility of scalability to large masses inherent to the structure of a TPC. A successful recent experiment that is taking advantage of these excellent properties is the XENON experiment [32] which aims the detection of WIMPs. It uses an LXeTPC that was upgraded from a 3kg detector to an intermediate 10kg detector [33], which in turn was upgraded to a 100kg apparatus. In the field of ββ0ν search, the EXO experiment is also using an LXeTPC, with 200kg of enriched gas [31] and the Gotthard experiment [35] used a 5kg high pressure gaseous xenon TPC (HPXeTPC). An LXeTPC has an obvious advantage over a HPXeTPC, which is the compactness of the detector. A smaller detector is less affected by external background such as the gammas emitted by the laboratory walls or by the detector vessel. Also, the density of liquid xenon is about 3g/cm^3 while the density of gaseous xenon at 10 bar is about 0.05 g/cm^3. Therefore, the primary scintillation yield is higher for liquid xenon than for gaseous xenon, and the detector will have an effect of self-shielding, since the gammas will interact near the detector wall. However, from the point of view of the observation of the signal topology, the high density of liquid xenon is a disadvantage.

The distinctive signature of a ββ0ν decay is the emission of two electrons whose sum of kinetic energies is equal to the $Q_{\beta\beta}$ value (2480 keV). These electrons will lose its energy mainly by inelastic collisions with the xenon atoms.

The collision mean energy loss of electrons per unit path length in a medium is described by the Bethe-Bloch Formula [36]:

$$-\left(\frac{dE}{dx}\right)_{col} \propto \rho \frac{Z}{A} \frac{z^2}{\beta^2} f(\beta, W_{max}, I, \delta, C) \qquad (8)$$

The electrons lose energy at a mean rate that is approximately proportional to the density of the medium. Therefore, these electrons will deposit all its energy in a blob in the liquid but, on the other hand, they are easily tracked in the gas because it is much less dense.

Figure 1.5 shows a Monte Carlo simulation of a ββ0ν event in a HPXeTPC at 10 bar. Each electron has an approximate energy of 1250 keV, and each of them will travel about 15 cm in the gas, depositing an energy of about 70 keV/cm, except for the end of the track where both electrons deposit about 200 keV. The resulting topological signature is a twisted track due to the multiple interactions of both electrons with the xenon atoms.

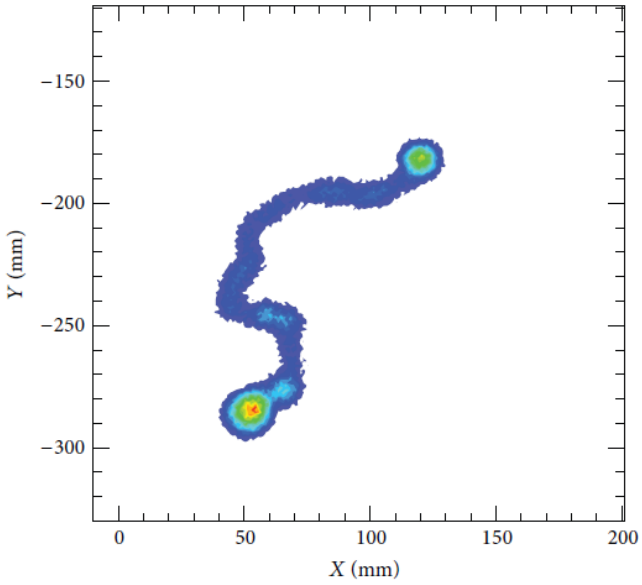

Figure 1.5. Monte Carlo simulation of the topology of a ββ event in HPXeTPC at 10 bar [13].

1.4. The NEXT Experiment

NEXT is an acronym for Neutrino Experiment with a Xenon TPC, and it is an international collaboration between several institutions. This experiment aims for the detection of ββ0ν signals using a detector named NEXT-100 that is being constructed in the Laboratorio Subterráneo de Canfranc (LSC) in Canfranc, Spain. It is an extension of the NEXT-DEMO prototype which is ten times smaller, and it is currently being operated in the Instituto de Física Corpuscular (IFIC) in Valencia, Spain.

1.4.1. Detector NEXT-100

The detector NEXT-100 will consist of a TPC filled with 100kg of gaseous xenon at high pressure, enriched at 90% of ^{136}Xe isotope.

This detector combines accurate energy measurements and 3D tracking techniques.

Figure 1.6 shows the main features of the NEXT-100 detector. The energy plane is placed behind the cathode and shall consist of an array of 60 photomultiplier tubes (PMTs) that will cover about 30% of the cathode area. The tracking plane is on the opposite side and will consist of an array of 7000 Silicon Photomultipliers (SiPMs). The electroluminescence region is 5 mm thick and is limited by two stainless steel meshes, placed few mm away from the tracking plane, Figure 1.7.

The chamber of the detector is covered with highly-reflective panels of Teflon. These panels will have the function of guiding the light to the photosensors with the highest possible efficiency.

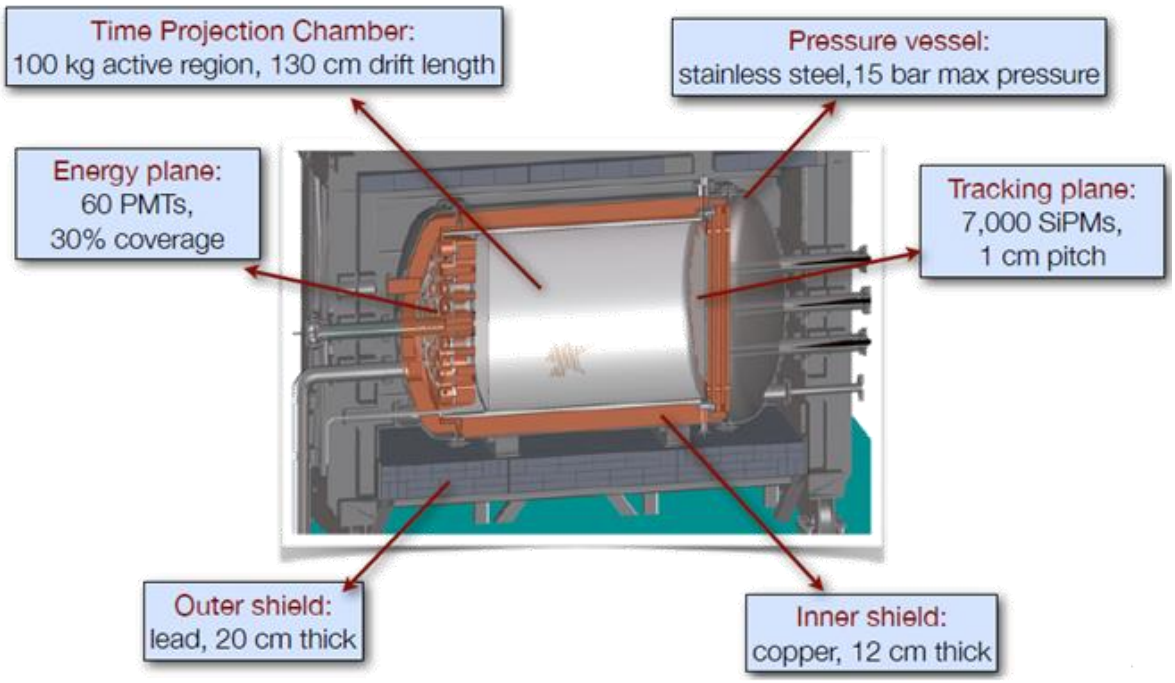

Figure 1.6. NEXT-100 detector main features [37].

1.4.2. The SOFT concept

SOFT is an acronym for Separated Optimized Functions for Tracking and is a concept used in the NEXT-100 detector that is represented in Figure 1.7.

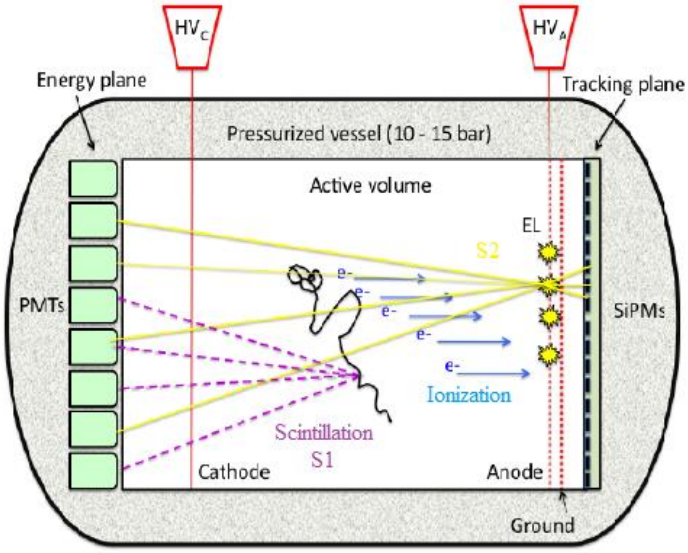

Figure 1.7. The Separate, Optimized Functions (SOFT) concept in the NEXT experiment. (modified from [38])

In this mode of detector operation the measurements of energy and tracking are performed separately.

A charged particle depositing energy in the detector will ionize and excite the xenon atoms producing a set of primary electrons and primary scintillation (S1) in the range of the vacuum ultraviolet (VUV) (172 nm). This primary scintillation is detected almost instantaneously by the PMTs in the energy plane, providing the initial time of the interaction, also known as the *start of event*.

The primary electrons will drift to the EL region under the influence of an electric field whose intensity is below the excitation threshold of the gas. In the EL region the intensity of the electric field is higher than the excitation potential of the gas, but lower than its ionization threshold. In this way, secondary scintillation, or electroluminescence, will be produced without electron avalanche multiplication, which would increase the statistical fluctuations and, hence, degrade the energy resolution. This scintillation is

emitted isotropically and about half of it will reach the tracking plane while the other half will be reflected by the detector walls and will reach the energy plane.

The EL region is so close to the tracking plane that the scintillation that will reach it will not disperse significantly, and the detection of this EL will provide information on the x- and y-coordinates of the event. The z-coordinate is obtained if the *start of event* time and the electron drift velocity in the gas are known. In this way, a 3D reconstruction of the event can be made.

In the energy plane the electroluminescence is converted into an amplified electrical signal and an accurate energy measurement is obtained.

The strong advantage of the SOFT concept is the fact that the optimization of the two planes can be done separately, since the two planes have distinct photosensors that need different gain proportions.

1.4.3. Drawbacks

Xenon is a slow gas with a large electron diffusion, factors that present a drawback for the 3D-tracking discrimination. Improvement of these parameters is, therefore, crucial for a most effective background reduction.

The addition of molecular additives to pure xenon will have a significant impact on the reduction of the primary electron cloud diffusion and on the increase of the electron drift velocity in the mixture. However, such additives will also lead to a reduction of the mixture's electroluminescence yield and to an increase of the statistical fluctuations associated with the electroluminescence production, since a collision between a drifting electron and a molecule may absorb the electron kinetic energy to vibrational and rotational states and, therefore, will not lead to electroluminescence production. Detailed research has to be performed to find the best compromise between the amount of molecular additive and the reduction of electroluminescence yield, or the increase of the statistical fluctuations associated to the EL production.

2. Gas Filled Detectors

2.1. Introduction

Gas filled detectors have all the same basic design, consisting of two electrodes, an anode and a cathode, separated by a gas. The gases used to fill the detector are usually pure noble gases or their mixtures.

Ionizing radiation passing through the gas can excite and/or ionize its atoms/molecules, if the energy deposited in the detector is higher than the excitation or ionization potential of the gas, respectively. The excited atoms can decay emitting scintillation, usually in the VUV range. This primary scintillation has a very low intensity, being difficult to detect. However, this primary scintillation is detected in certain experiments for the trigger or *start of event*.

The ions and electrons created in the ionization process are guided in opposite directions, under the influence of an electric field applied to the detector. This results in an electrical signal that can be collected by a suitable device coupled to the detector. This signal is proportional to the energy deposited in the detector and, hence, to the energy of the incident radiation.

If the signal generated by the thermalization of the primary electrons is well above the background of the experiment (electronic noise), it can be directly collected with no further amplification. In this case, the gas medium acts as a scintillator. An electric field below the gas excitation threshold is applied to guide the primary electrons towards the anode for further signal processing, if necessary.

In other cases, the number of primary electrons produced is so low that the corresponding signal cannot be distinguished from the electronic/background noise. Therefore, the output signal has to be amplified and the electrons will have to drift to a region of the detector where the applied electric field is significantly higher. If the electric field is higher than the ionization threshold of the gas, the electrons gain from it enough energy to ionize the gas atoms, producing an electron avalanche.

Charge avalanche amplification and collection is a straightforward process, but suffers of significant statistical fluctuations, as will be discussed in section 2.5.2.

Another type of amplification may be achieved through electroluminescence processes (gas scintillation through electron impact) without charge amplification. The statistical fluctuations associated to this process are negligible when compared to those associated with the primary electron cloud formation. In this case, the primary electrons are guided to a region where the applied electric field is above the gas excitation threshold but below its ionization threshold. The electrons gain enough energy from the electric field to further excite but not ionize the gas atoms, leading to the emission of VUV photons, as a consequence of the gas de-excitation. This will be discussed in section 2.4. A single electron can produce hundreds of photons.

On the other hand, this signal amplification alternative needs a suitable photosensor to convert the scintillation pulse into an electrical signal. The amplitude of this signal is proportional to the number of primary electrons, and hence, to the energy deposited in the detector by the incident radiation.

As an example, the Proportional Counter (PC) [36] uses electron multiplication as a way of signal amplification, while the GPSC uses electroluminescence for signal amplification.

2.2. Ionization in Gases

An ionizing particle passing through gas interacts with its molecules, creating both excited and ionized molecules, through a process that depends on the nature and energy of the particle. The interaction between the particle and the molecules of the medium are random and they are characterized by λ, the mean free path, which is defined as [39]:

$$\lambda = \frac{1}{n\sigma} \tag{9}$$

where n is the density of the molecules in the gas and σ is the effective cross section of the particle in the gaseous medium. The number of interactions along a certain path follows a Poisson distribution.

When an incident ionizing particle interacts with an atom transferring enough energy to ionize it, a bound electron can be ejected, and an electron-ion pair is created. The

energy of this ejected electron will depend on its binding energy and on the energy of the incident ionizing particle. If this ejected electron has enough energy, it can further ionize the gas. In this case, electrons will be produced until the energy available is below the ionization potential of the gas atoms (Figure 2.1).

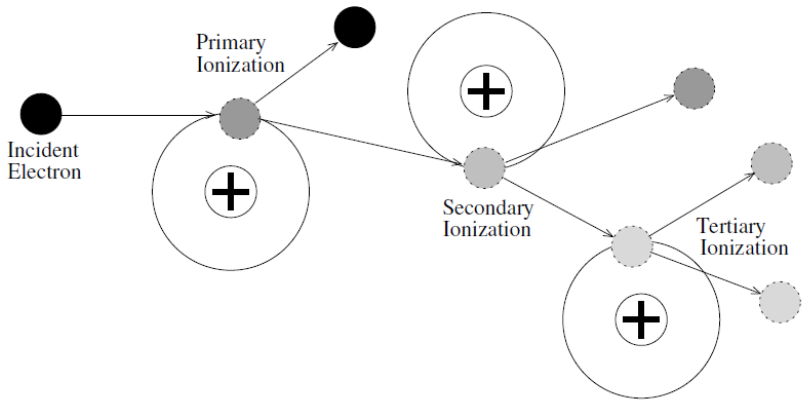

Figure 2.1. Ionization processes induced by electron interactions [39].

The needed average energy to produce an electron-ion pair is given by the w-value. This energy is significantly higher than the first ionization potential of the gas, since there is a non-negligible amount of energy spent in atom excitation.

For a particle that deposits a certain energy E in the detector, the w-value can be used to determine the mean number of primary electrons produced, N:

$$N = \frac{E}{w} \tag{10}$$

There are statistical fluctuations associated to the production of primary electrons and, therefore, this number is not always the same. If the ionizations are independent of each other, these fluctuations are described by a Poisson process. In this case, the variance would be given by:

$$\sigma_P^2 = N_e \tag{11}$$

However, this is not the case. It was empirically demonstrated that these processes of charge production are not independent, and the value of the observed variance, σ_e^2, is lower than that predicted by the Poisson distribution.

In 1947, the Italian American physicist Ugo Fano introduced the *Fano factor* [40], which is defined as the ratio between the observed variance, and the variance predicted by the Poisson model:

$$F = \frac{\sigma_e^2}{\sigma_P^2} \tag{12}$$

The value of the Fano factor is in the range between 0 (no fluctuations) and 1 (perfect Poisson process).

2.3. Transport of electrons in gases

The electrons and ions produced in the gas will collide multiple times with the gas atoms/molecules, losing part of their energy.

The ions are heavy particles and will lose a great amount of energy between collisions and are only slightly accelerated. For this reason, they will drift in the gas following the lines of the electric field with only small thermal fluctuations.

Electrons are much lighter than ions and will lose just a small fraction of their energy when they elastically collide with the gas molecules. Consequently, their drift velocity is much higher than that of the ions, approximately 1000 times higher. That is one of the reasons why in the majority of the applications only the signal from electrons is used.

2.3.1. Diffusion, recombination and attachment

The direction of motion of an electron can be abruptly changed after a collision. The most part of the electrons produced will follow the direction of the electric field lines (longitudinal direction). However, some of them will diffuse transversely. An electron

cloud drifting under the influence of an electron field spreads into a Gaussian spatial distribution whose standard deviation will increase with time, t, and it is given by [39]:

$$\sigma = \sqrt{2Dt} \tag{13}$$

where D is the diffusion coefficient.

Upon collisions with the positive ions, the electrons can be captured by them, forming a neutral atom or molecule in a process called *recombination*. Thus, these electrons will not contribute to the electrical signal collected in the anode. The rate at which this recombination processes occur is proportional to the concentration of electrons, n^-, and the concentration of positive ions, n^+, and can be defined using the recombination coefficient, α_{rec}:

$$\frac{dn^-}{dt} = \frac{dn^+}{dt} = -\alpha_{rec} n^- n^+ \tag{14}$$

There are two processes of recombination: *initial recombination* and *general recombination*. Initial recombination occurs when the electrons are captured by the ions in the same region where they were produced. This effect can be reduced by applying an electric field that will induce the ions and electrons to drift away from each other in opposite directions. General recombination occurs anywhere in the gas volume when positive ions and electrons encounter each other on their way to the cathode and the anode, respectively. The probability of this type of recombination to occur is dependent on the density of positive ions and electrons.

The detector medium can contain impurities. The electrons drifting in the gas can collide with these impurities resulting in the *attachment* to the neutral atom or molecule. This process will contribute to the degradation of the detector performance, since these lost electrons will not contribute to the overall electrical signal.

2.4. Electroluminescence in Noble Gases

The detector used in this work was a GPSC and among the noble gases, xenon is the one that presents better conditions to be the filling gas for this detector. It has a high absorption cross section for x-rays, a high scintillation efficiency and also a high electroluminescence yield.

The scintillation mechanism that occurs during the electroluminescence process can be described by the following expressions:

$$\begin{aligned} X + e &\rightarrow X^* + e \\ X^* + 2X &\rightarrow X_2^* + X \\ X_2^* &\rightarrow 2X + h\nu \end{aligned} \tag{15}$$

From the collisions between the electrons and the noble gas atoms result atoms in the excited states X*. Due to their long lifetime and to the high number of collisions with atoms in the ground state, it is probable that a three body collision will occur, which results in the production of excimers that than will de-excite to the ground state emitting VUV photons [41].

2.5. Gas Proportional Scintillation Counter

GPSCs are gaseous detectors that had been used in areas such as x-ray spectroscopy, medical instrumentation, astrophysics, among other applications. Its origin can be connected to the pioneer investigation works of Professor Carlos Conde and Professor Armando Policarpo [42].

There are GPSCs with many geometries and configurations. The uniform field geometry of the GPSC is the most commonly used and will be the one discussed in this section. A scheme of this detector is represented in Figure 2.2.

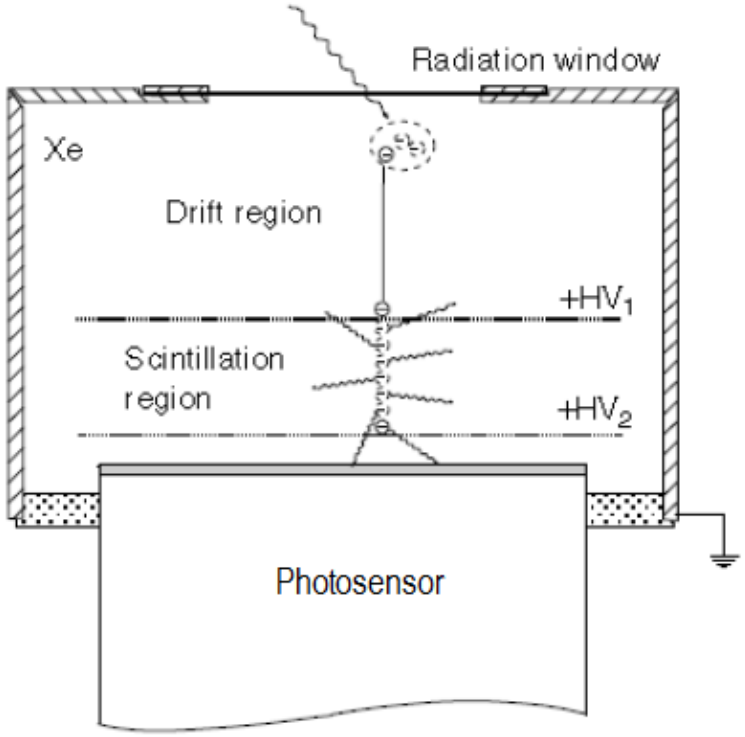

Figure 2.2. Scheme of the standard uniform field GPSC (modified from [43]).

As can be seen in Figure 2.2, the uniform field GPSC is divided in 3 regions.

The first region is the *drift region*, where the incident ionizing radiation is absorbed by the gas. The gas atoms can be excited and ionized, leading to the production of primary scintillation and to a primary electron cloud, respectively. If these electrons have energy above the excitation threshold or the ionization threshold of the gas, further excitation and ionization will occur, until the energy of the electrons is below these thresholds. The

number of primary electrons produced is approximately proportional to the energy of the absorbed radiation. Normally, the filling gas is a noble gas or a mixture of noble gases, and the emitted radiation has wavelengths in the range of the VUV. In the majority of applications this first scintillation is not used because it has a very low intensity and is very difficult to detect for low-energy incident particles.

In the drift region an electric field is applied with intensity lower than the excitation threshold of the filling gas. The primary electrons will drift, under the influence of this electric field, to the second region of the detector, the *scintillation region*.

The intensity of the electric field applied to the scintillation region is higher than the excitation threshold of the gas, but lower than its ionization threshold. The primary electrons acquire in this region enough energy to excite the gas atoms. In the de-excitation process they emit VUV photons, the secondary scintillation or electroluminescence (EL). The amount of EL produced is proportional to the energy of the incident radiation, which has given the name to the Gas Proportional Scintillation Counter (GPSC).

The third region of the detector is the *photosensor*, which converts the EL in an electric signal. The most commonly used photosensors are the Photomultiplier Tube (PMT) or the Avalanche Photodiode (APD).

2.5.1. Uniform Electric Field Driftless GPSC

In the driftless GPSC there is no drift region and the x-rays are absorbed directly in the scintillation region. In this configuration, the amount of secondary scintillation that will be produced by the interaction of the x-rays with the gas medium will depend on the position where the interaction occurs and, thus, on the distance travelled by the primary electron cloud in the detector volume. Since the scintillation pulse duration is proportional to this distance the proportionality between the signal amplitude and the incident x-ray energy can be re-established by normalizing the drift times.

This correction does not have to be applied to soft x-rays, due to the fact that its penetration depth is low compared to the thickness of the scintillation region, and the distance travelled by the primary electron cloud in the scintillation region will be basically the same [43].

Figure 2.3 shows typical pulse-height distributions obtained using a standard GPSC and a Driftless GPSC, respectively. The signal of the standard GPSC is symmetric, having a Gaussian shape. In the other case, there is a deviation from this symmetric behaviour, with the appearance of a tail in the low-energy region.

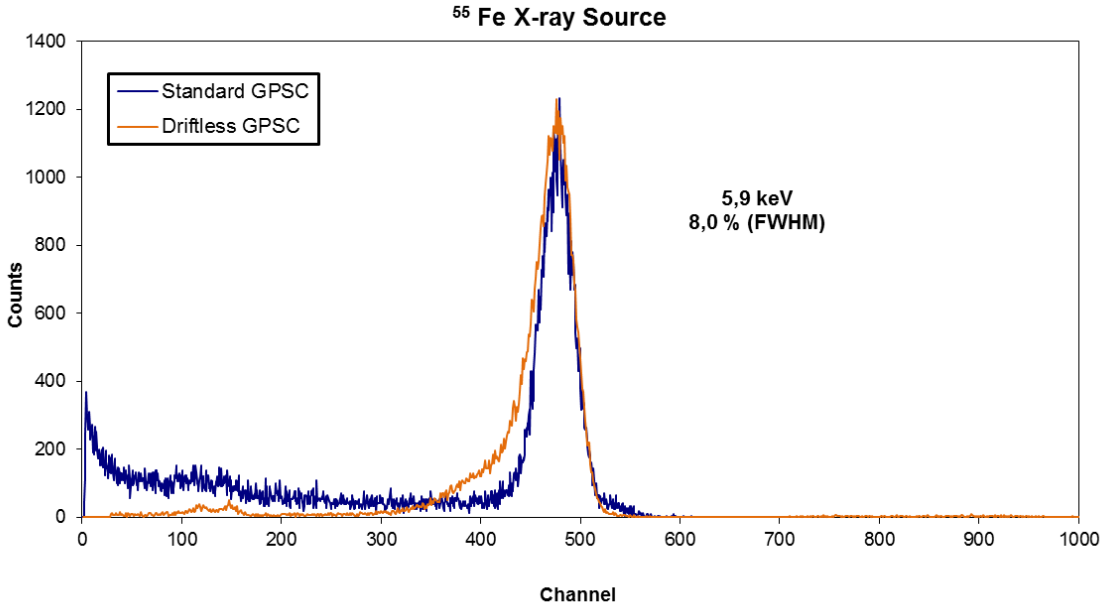

Figure 2.3. Typical spectrums obtained with a Standard GPSC (blue), with a PMT bias voltage of 690V, E/p in the drift region of 0.6 V/cm/torr and in the scintillation region of 5.0V/cm/torr, and with a Driftless GPSC (orange), with a PMT bias voltage of 650V and an E/p of 4.5V/cm/torr.

The pulse-height distribution for the driftless GPSC was obtained with the experimental setup used in this work, whereas the one obtained for the standard GPSC was obtained with a detector coupled to a R8520-06SEL Hamamatsu PMT and with a 3-cm thick drift region and a scintillation gap of 0.5 cm.

We have used a driftless GPSC to minimize the effect of attachment, reducing the path length and applying a strong electric field along this path, and to minimize the scintillation quenching, reducing the detector dimensions. Both effects, attachment and scintillation quenching, would interfere with the results to be obtained in this work.

2.5.2. Energy Resolution of a GPSC

One important property of a detector in radiation spectroscopy is its response to a monoenergetic source of radiation.

The energy resolution of a detector is defined as the ratio between the FWHM (full-width-at-half-maximum) and the centroid of the pulse-height distribution. The larger the width of the distribution, the higher the amount of fluctuations that occur for the same amount of energy deposited in the detector, for each event [36].

For a detector with signal amplification based on *electron avalanche* there are fluctuations inherent to the number of primary electrons produced and to the avalanche multiplication. For example, the energy resolution for PCs is given by [36]:

$$\mathrm{R(FWHM)\%} = 2.355\sqrt{\frac{\mathrm{w}}{\mathrm{E}}(\mathrm{F}+\mathrm{f})} \tag{16}$$

where the *w*-value is the average energy needed to produce an electron-ion pair, E is the energy deposited in the gas by the incident particle, F is the Fano factor and *f* is the parameter that describes the statistical fluctuations inherent to single electron multiplication and is usually much larger than F, being the largest parameter in the energy resolution of this type of detectors.

For detectors based on the electroluminescence, as is the case of the GPSC, there are statistical fluctuations inherent to the number of primary electrons produced, given by F, fluctuations in the number of photons produced per primary electron, given by J, and fluctuations inherent to the photosensor . J is equal to the ratio between the variance in the number of emitted photons per primary electron, and the variance if the process were described by the Poisson model (average number of photons per primary electron). J is usually much lower than F. The energy resolution of a GPSC can be given by [43],

$$\mathrm{R(FWHM)\%} = 2.355\sqrt{\frac{\mathrm{F}}{\mathrm{N}}+\frac{1}{\mathrm{N}}\left(\frac{\mathrm{J}}{\mathrm{N_S}}\right)+\left(\left(\frac{\sigma_{\mathrm{N_e}}}{\mathrm{N_e}}\right)^2+\frac{1}{\mathrm{N_e}}\left(\frac{\sigma_{\mathrm{q}}}{\mathrm{G_q}}\right)^2\right)} \tag{17}$$

where N is the average number of primary electrons produced per incident x-ray, F is the relative variance of N, the Fano factor, N_S is the average number of scintillation photons produced per primary electron, J is the relative variance of N_S, $(\sigma_{N_e}/N_e)^2$ is the relative variance in the number of photoelectrons produced in the PMT per x-ray interaction, N_e, $(\sigma_q/G_q)^2$ are the fluctuations in the electron multiplication gain of the photosensor. Other contributions, e.g. of geometric nature, as those due to variations in the solid angle subtended by the PMT photocathode relative to the region where the scintillation occurred and electronic noise, are not taken into account in Eq. (17).

The second term under the radical of Eq. (17) can be neglected since $J \ll F$ and $Ns > 100$. The number of primary electrons produced in an x-ray interaction is given by the energy of the x-ray divided by the mean energy to produce one electron-ion pair, Eq. (10). As the photoelectron production is a Poisson process, while the gain of each photoelectron in the PMT avalanche approaches an exponential distribution, the energy resolution of the GPSC can be approximated to [44] :

$$R(FWHM)\% = 2.355\sqrt{\frac{Fw}{E_x} + \frac{2}{N_e}} \tag{18}$$

3. Driftless GPSC Operation Principles and Performance

3.1. Introduction

As was said before, in a driftless GPSC [45], the x-ray interaction takes place directly in the scintillation region and this configuration was chosen to minimize any effect of electron attachment and scintillation quenching, which could hinder the effect of the additive on the electroluminescence yield of the mixture, parameter to be measured in this work.

Figure 3.1 shows a typical pulse-height distribution obtained for pure xenon and for 5.9-keV x-rays. The pulse-height distribution presents the typical Gaussian shape convoluted with an exponential tail towards the low-energy region, due to the x-ray penetration in the scintillation region. For 5.9-keV x-rays this tail is small, given its small absorption length in xenon, 2.7 mm at 1 bar, when compared to the thickness of the scintillation region, 25 mm. Therefore, for centroid as well as for FWHM measurements, only the right part of the distribution was fit to a Gaussian function, from which the centroid and the full-width-at-half-maximum were taken.

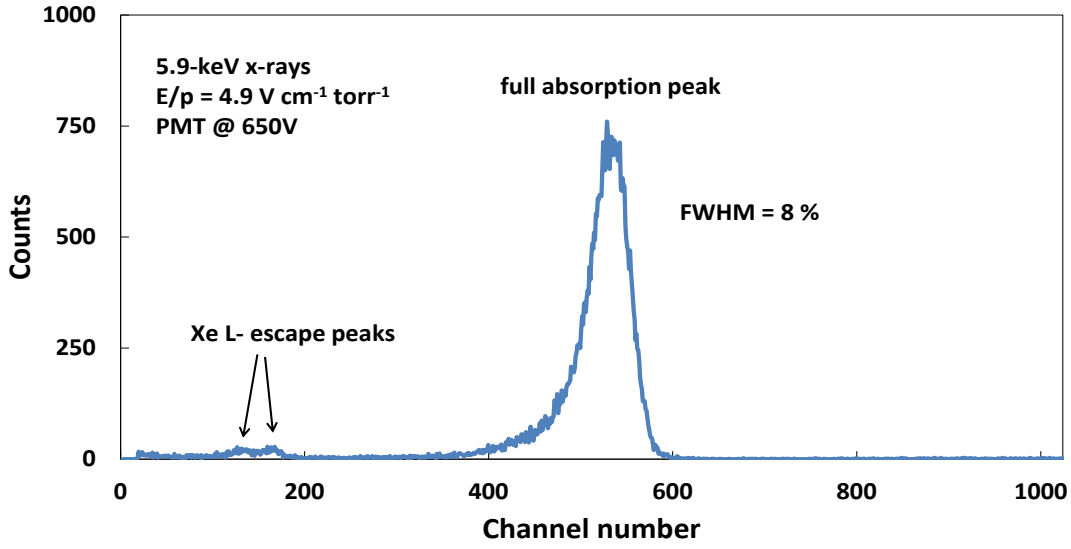

Figure 3.1. Pulse-height distribution for 5.9-keV X-rays absorbed in the xenon driftless GPSC. The PMT was biased at 650 V, the reduced electric field was 4.9 V/cm/ torr-1 and shaping constants were 5 μs.

Figure 3.2 presents a typical behaviour of electroluminescence relative amplitude and energy resolution as a function of reduced electric field, E/p, for a xenon filled GPSC. The amplitude exhibits a linear dependence on the reduced electric field in the scintillation region, with an intercept around 1.0 V/cm/torr (xenon excitation threshold), in agreement with the values reported in the literature [43]. For low E/p values, the energy resolution presents a fast decrease with increasing E/p in the scintillation region due to the strong increase in the amount of electroluminescence produced, stabilizing for high reduced electric fields, as the electroluminescence reaches levels high enough for the statistical fluctuations inherent to the scintillation processes to become negligible.

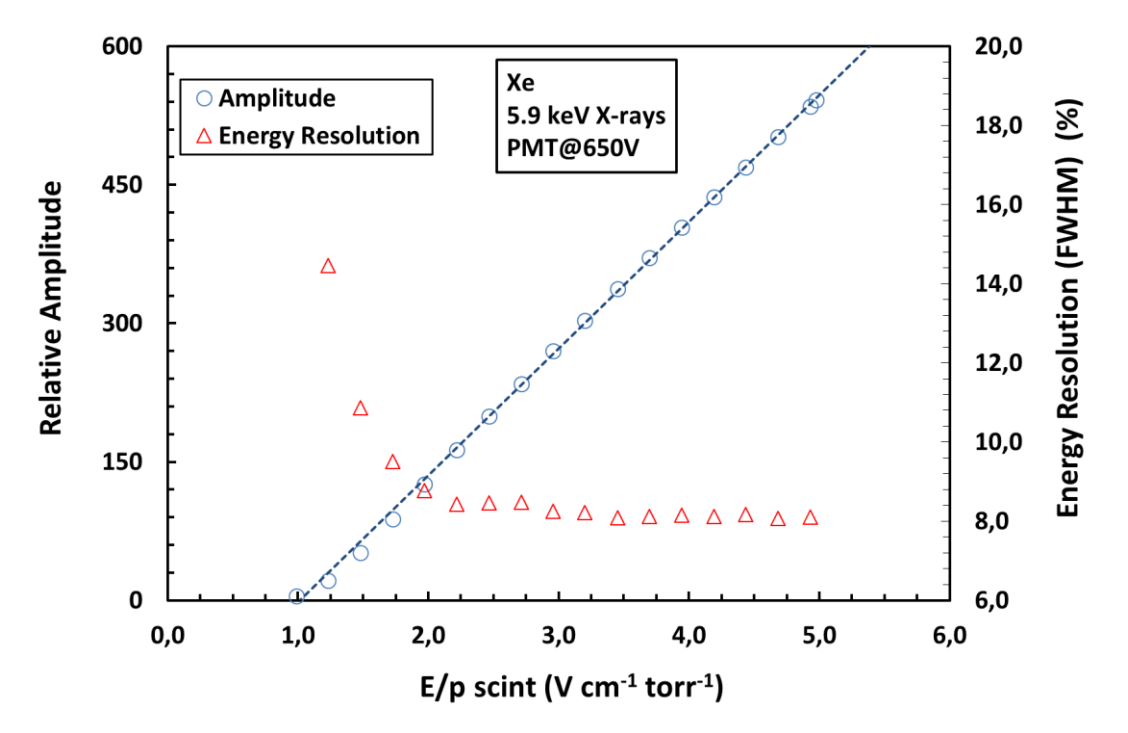

Figure 3.2. Relative amplitude and energy resolution (FWHM) as a function of reduced electric field, E/p, for pure xenon, for 5 μs shaping constants. A PMT bias voltage of 650 V was used and the gas pressure was 800 torr.

3.2. Experimental Setup

The detector used in this work [43][45] has 10 cm in diameter and a 2.5-cm deep scintillation region, filled with Xe or Xe-CO_2 mixtures at pressures close to 1 bar. It was continuously purified through SAES St-707 getters that were kept at a temperature of 80^0C to avoid the absorption of CO_2. The upper part of the detector body is made of Macor, which insulates the 8-mm in diameter Kapton radiation window and its stainless steel holder. Kapton, stainless steel and Macor were epoxied to each other. The Kapton window is aluminised on the inner side to ensure electrical conductivity. The lower part of the detector is made of stainless steel and connected to the gas circulation system. The bottom of the detector is a Macor disc epoxied to a 51-mm in diameter PMT and to the detector wall. The PMT is an EMI D676QB (an 8-dynode version of the EMI 9266QB PMT). A chromium grid with a line width of ~100 μm and 1000 μm spacing was vacuum-deposited onto the PMT quartz window and connected to the photocathode pin through a continuous chromium film deposited on the side surface. The upper and lower parts of the detector were vacuum-tight by compression of an indium gasket.

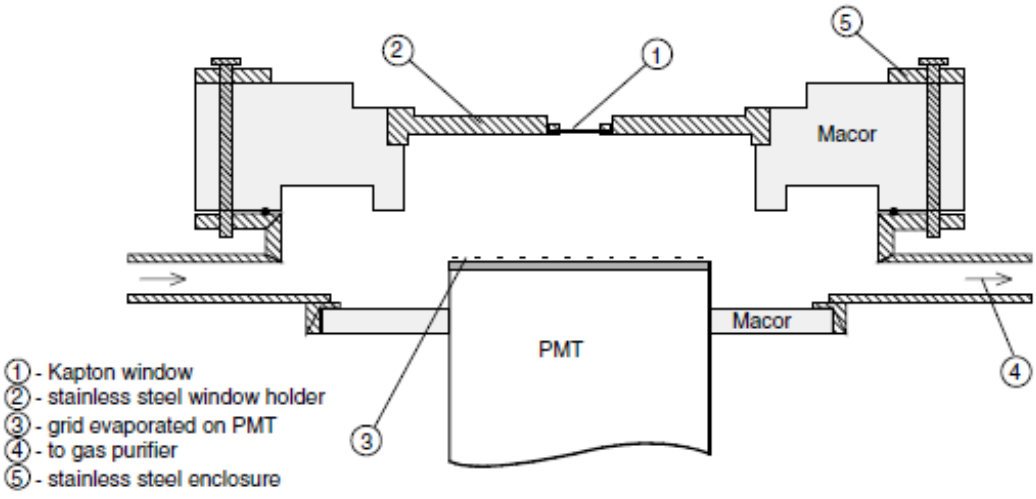

Figure 3.3. Scheme of the driftless GPSC used in this work [45].

The Kapton window and holder were kept at negative high voltage, while the chromium grid and PMT photocathode were kept at 0 V. The window holder and the

upper Macor piece were designed to ensure a uniform electric field in the scintillation region.

The charge signal from the PMT was pre-amplified with a Canberra 2004 preamplifier, with sensitivity of 9 mV/MeV and, subsequently, formatted with a HP 5582A linear amplifier, using integration /differentiation constants of 5 μs and 50 ns. The formatted pulses were collected with a 1024-channel multichannel analyser (MCA). By using 5 μs shaping constant, we ensure that the collected signal corresponds to the total amount of EL produced in the entire scintillation region.

The detector was irradiated with a 5.9-keV x-ray beam from a ^{55}Fe radioactive source. A thin chromium film, placed between the radioactive source and the detector radiation window, absorbs most of the 6.4-keV x-rays of the Mn K_β line of the ^{55}Fe source.

The different gas mixtures were achieved by adding known volumes filled with pure CO_2 at known pressures to the xenon in the main detector chamber.

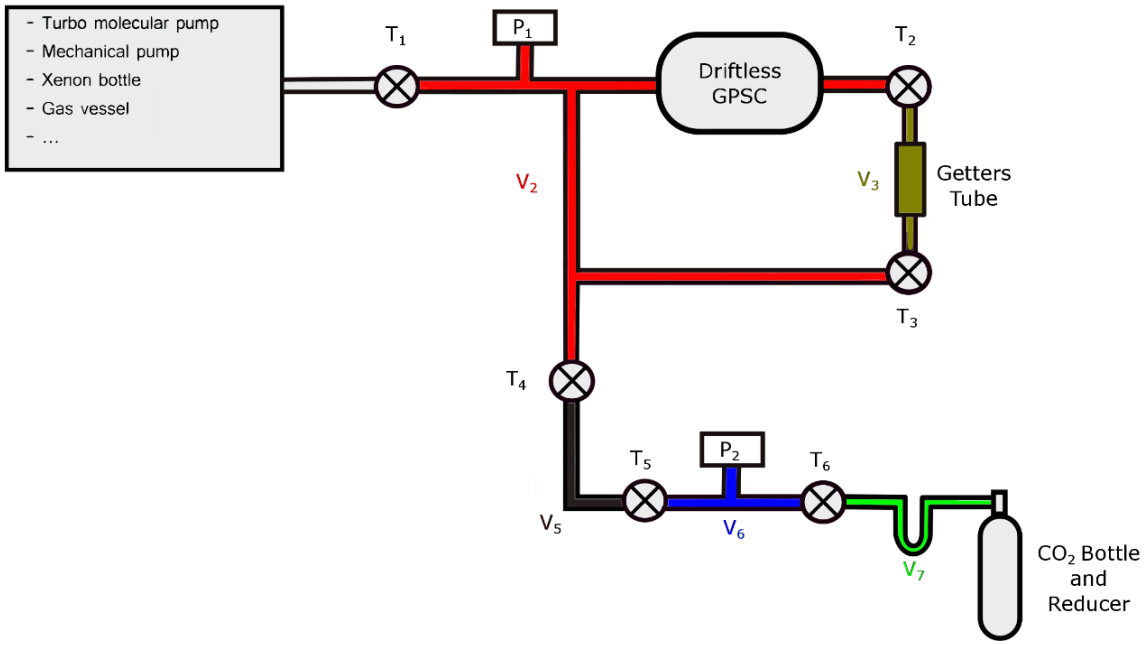

Figure 3.4. Scheme of both gas systems connected to the detector.

3.2.1. Ratio between the partial volumes of the system

In this section is showed how to calculate the ratio of the different volumes that constitute the detector gas and impurities systems (see Figure 3.4). The knowledge of the relations between these volumes is essential to have an accurate measure of the percentage quantity of CO_2 added to the pure xenon in the detector.

Considering that $\mathbf{V_1}$ is the **total volume of the main detector chamber + circulation tubes**, i.e, the detector gas system, and it is divided in two volumes, V_2 and V_3:

- $\mathbf{V_2}$ is the total volume of the main detector chamber without the getters' tube.
- $\mathbf{V_3}$ is the volume of the getters' system, between valves T_2 and T_3.

$$\mathbf{V_1 = V_2 + V_3} \tag{19}$$

$\mathbf{V_4}$ is the **total volume of the impurities system** that is divided in three volumes, V_5, V_6 and V_7:

- $\mathbf{V_5}$ is the volume between valves T_4 and T_5.
- $\mathbf{V_6}$ is the volume between valves T_5 and T_6.
- $\mathbf{V_7}$ is the volume between valve T_6 and the CO_2 bottle.

$$\mathbf{V_4 = V_5 + V_6 + V_7} \tag{20}$$

The relations between all of these volumes can be measured using the ideal gas law, $PV = nRT$, keeping constant the number of moles, n, and the temperature, T.

The procedure to determine these relations was as follows:

1) T_2, T_3 and T_4 valves were closed (impurity system and getters' tube closed);
2) V_2 was filled with a certain amount of gas;
3) T_2 and T_3 valves were opened, and the pressure in V_2+V_3 was measured.
4) Using $P_iV_i=P_fV_f$:

$$P_{i2}V_2 + P_{i3}V_3 = P_f\,(V_2+V_3) \tag{21}$$

where P_{i2} and P_{i3} are the initial pressures in volumes V_2 and V_3, respectively, and P_f is the final pressure in volume V_2+V_3. The variables P_{i2}, P_{i3} and P_f are known. Note that P_{i3}= 0 torr, therefore:

$$V_2 = \frac{P_f}{P_{i2} - P_f} V_3 \tag{22}$$

Hence, the relation between the volumes V_2 and V_3 was found. Following similar procedures for other volumes and performing the calculations, the following relations were found:

$$V_1 = 68.51V_5 \tag{23}$$

$$V_1 = 1.15V_2 \tag{24}$$

$$V_2 = 6.74V_3 \tag{25}$$

$$V_6 = 2.42V_5 \tag{26}$$

$$V_2 = 59.57V_5 \tag{27}$$

With the knowledge of these volume relations one can estimate the quantity of CO_2 that should be added to the xenon, in order to achieve the percentages of molecular additive to be studied.

As an example, considering that:

1) Valves T_1 and T_4 are closed.
2) V_1 is filled with pure xenon at a pressure $P_{Xe(V1)}$.
3) V_4 contains a pressure of CO_2 above the atmospheric pressure.

For instance, a mixture of x%Xe+y%CO_2 needs to be studied. The detector gas system (volume V1) is already full with pure xenon at $P_{Xe(V1)}$. It is necessary to calculate the initial pressure of CO_2 needed in volume V_5 so that, when valve T_4 is opened, we have a specific partial pressure of CO_2 in volume V_1+V_5, and this partial pressure of CO_2 is around y% of the total gas mixture in volume V_1+V_5. First, one has to calculate the partial pressure of Xe, P_{Xe}, in volume V_1+V_5 after T_4 valve is opened:

$$P_{Xe(V_1)}.V_1 + P_{Xe(V_5).}V_5 = P_{Xe}.(V_1 + V_5) \quad (28)$$

Substituting Eq.(23) in Eq.(27), and noting that $P_{Xe(V5)} = 0$:

$$P_{Xe} = \frac{68.51}{69.51} P_{Xe(V_1)} \quad (29)$$

The total pressure, P_T, in the volume V_1+V_5 will be equal to the partial pressure of Xe, P_{Xe}, plus the partial pressure of CO_2, P_{CO2}, in the same volume:

$$P_T = P_{Xe} + P_{CO_2} \quad (30)$$

This partial pressure of CO_2 in V_1+V_5 will be related to the pressure of CO_2 in V_5 through the follow relation:

$$P_{CO_2(V_1)}.V_1 + P_{CO_2(V_5).}V_5 = P_{CO_2}.(V_1 + V_5) \Leftrightarrow$$

Noting that $P_{CO2(V1)} = 0$:

$$\Leftrightarrow P_{CO_2} = \frac{1}{69.51} P_{CO_2(V_5)} \quad (31)$$

Substituting Eq.(28) and Eq.(30) in Eq.(29):

$$P_T = \frac{68.51}{69.51} P_{Xe(V_1)} + \frac{1}{69.51} P_{CO_2(V_5)} \quad (32)$$

The percentage of CO_2 present in the final mixture is given by:

$$(y\%)_{CO_2} = \frac{P_{CO_2}}{P_T} \times 100 \quad (33)$$

Therefore, using the above equations, one can know the pressure of CO_2 needed in V_5 to achieve a certain percentage of this molecular additive in the final mixture:

$$P_{CO_2(V_5)} = 68.51 P_{Xe(V_1)} \frac{(y\%)_{CO_2}}{100 - (y\%)_{CO_2}} \quad (34)$$

After knowing the initial pressure of CO_2 in volume V_5, and with the help of liquid nitrogen and the U tube found in Volume V_7, one can collect all of the CO_2 present in volume V_4 and, after withdrawing the liquid nitrogen, slowly, reach the needed pressure value.

After the mixture is done, the nominal value of y achieved can be improved, after reading the final total pressure, P_T, in volume V_1+V_5, with a certain precision in P_1. Calculations can be redone and a more accurate value of y can be achieved.

3.3. Experimental Results

In this section the study of the performance of the detector with pure xenon is presented. This study was done in order to verify the good performance of the detector.

3.3.1. Performance of the Detector with Pure Xenon

The first step was to make vacuum in the detector chamber, in the gas circulation tubes and in the CO_2 filling system. A pressure at the order of the 10^{-6} mbar was reached near the turbo pump.

Afterwards, *reactivation of the getters* [46] was performed for correct purification of the gaseous xenon. The temperature of the getters was increased from 25ºC to 375ºC, in steps of about 40ºC, through the use of a heating tape. As the temperature was being increased the getters started to expel impurities such as H, O, among others. Consequently, the pressure in the whole system increased. Since the pumping system was still working, these impurities were cleaned out from the system and the pressure began to decrease for a certain time until it stabilized. When the pressure stabilized the temperature was again increased and the same procedure was used repeatedly until the temperature of 375ºC was reached. At 375ºC the getters had expelled all the impurities and this temperature was kept constant for about an hour, in order for the getters to be operational at 90%-100% [46].

After that hour a pressure similar to the initial one was reached. To verify if the getters were operational, the valves T_2 and T_3 were closed. As a consequence, the pressure in the whole system increased without the pumping action of the getters. Subsequently, the valves were opened and the pressure decreased. Since the pressure increased when the getters' system was not operating, and decreased when it was operating, one could conclude that the getters were purifying the gas properly.

The xenon bottle used to provide the required gas to the main detector chamber is located in the main vacuum system lines. In the same system an empty bottle was placed,

and this bottle is represented as *gas vessel*. This gas vessel was used to collect xenon and to purify it from water molecules and other impurities which were trapped in the gas vessel by using liquid nitrogen on the outer surface of the gas vessel.

The pumping system was closed, the xenon bottle was opened, the gas vessel was opened and liquid nitrogen was used to collect the xenon. When all the xenon was collected in the gas vessel, the liquid nitrogen was removed and T_1 valve was opened, with T_4 closed. The gas vessel was heated in order to accelerate the process of separation of the xenon from the impurities. The detector was filled with xenon at approximately 800 torr and T_1 was closed again. The xenon circulating in the main vacuum system lines was collected in the gas vessel using liquid nitrogen. The pumping system was opened to clean the main vacuum system lines until a pressure of about 10^{-6} mbar was reached.

The temperature of the getters was lowered to 180ºC and kept at this value for one day. Afterwards, the temperature was lowered to 80ºC, and the studies were carried out at this temperature.

The performance of the detector was tested at 80ºC. Figure 3.5 shows the relative amplitude and energy resolution obtained as a function of reduced electric field, for integration/differentiation constants of 5 us.

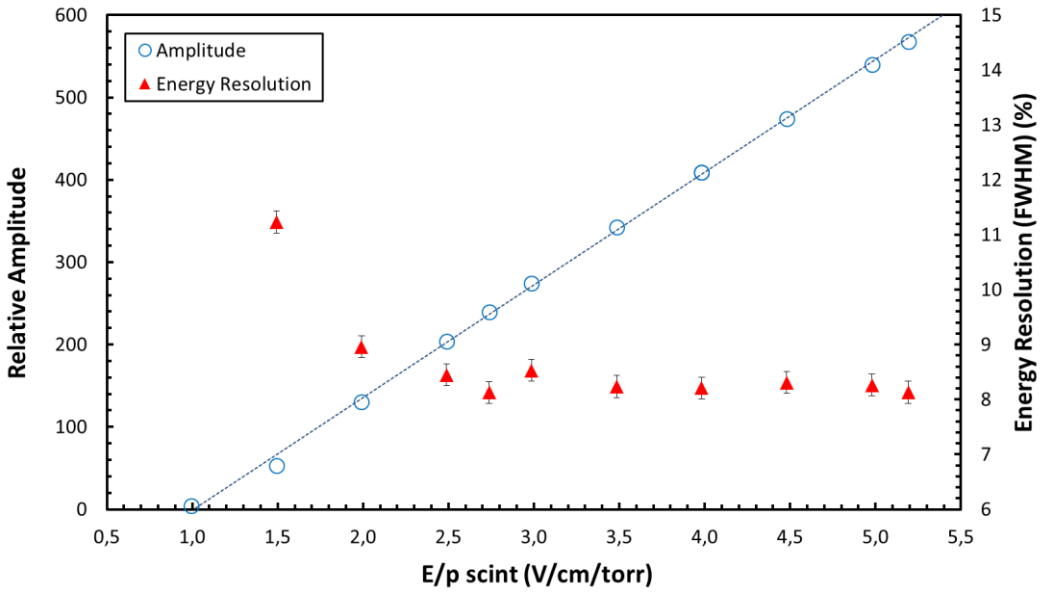

Figure 3.5. Relative amplitude and energy resolution (FWHM) as a function of reduced electric field, E/p, for pure xenon, with getters operating at 80ºC, for 5 μs shaping constants. A PMT bias voltage of 650 V was used and the gas pressure was about 790 torr.

As seen in Figure 3.5 the electroluminescence relative amplitude exhibits a linear dependence on the reduced electric field in the scintillation region, and intercepts the x axis around 1.0 V/cm/torr. For low E/p values, the energy resolution presents a fast decrease with increasing E/p in the scintillation region, stabilizing for high reduced electric fields. This behaviour of both relative amplitude and energy resolution for the different reduced electric field values is in agreement with the results set forth in section 3.1. The detector exhibited a good performance to be used in the studies of the Xe - CO_2 mixtures.

4. Study of Xe-CO_2 Mixtures

4.1. Introduction

Experimental studies of Xe-CH_4 mixtures have shown that it is possible to add small concentrations of molecular additives to xenon without significant loss of electroluminescence yield. CO_2 would be an interesting option due to its low cost and easy handling. In addition, simulation results of diffusion in Xe-CO_2 mixtures have shown that concentrations of the order of 0.1%-0.2% of CO_2 would be sufficient to reduce transversal and longitudinal diffusion to acceptable values. The effect of the addition of CO_2 to pure xenon is not referred in the literature and, on the other hand, it has always been assumed that the presence of CO_2 impurities is a strong killer of electroluminescence. Nevertheless, the same assumption had been made for CH_4, which our group proved in former studies to be an acceptable additive, in Xe-CH_4 mixtures for CH_4 concentrations lower than 0.5% - 1% [44].

In this way, we have studied the impact of the addition of a nominal value of 0.11%, 0.33% and 0.5% of CO_2 to pure xenon on the electroluminescence yield and on the energy resolution achievable with these mixtures. A comparison is made with the results for pure xenon.

4.2. Mixture of 99.89% Xe+0.11% CO_2

Figure 4.1 shows the variation with time of the electroluminescence relative amplitude as a function of reduced electric field, when 0.11% of CO_2 was added to xenon, and the getters operation temperature was 80ºC. The excitation threshold is close to the one of pure xenon (1.0 V/cm/torr). The mixture was stable for a long period of time.

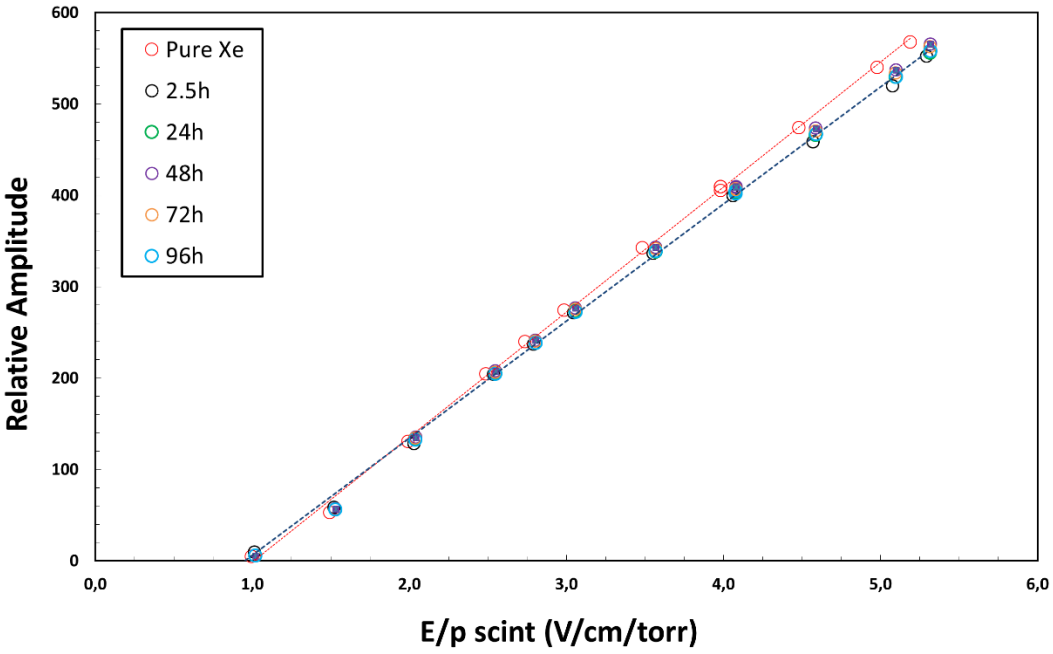

Figure 4.1. Relative amplitude as a function of reduced electric field, E/p, for the mixture of 99.89% Xe+0.11% CO_2 at 80°C with a filling pressure of 750 torr, for a constant PMT bias voltage of 650 V and shaping constants of 5 μs.

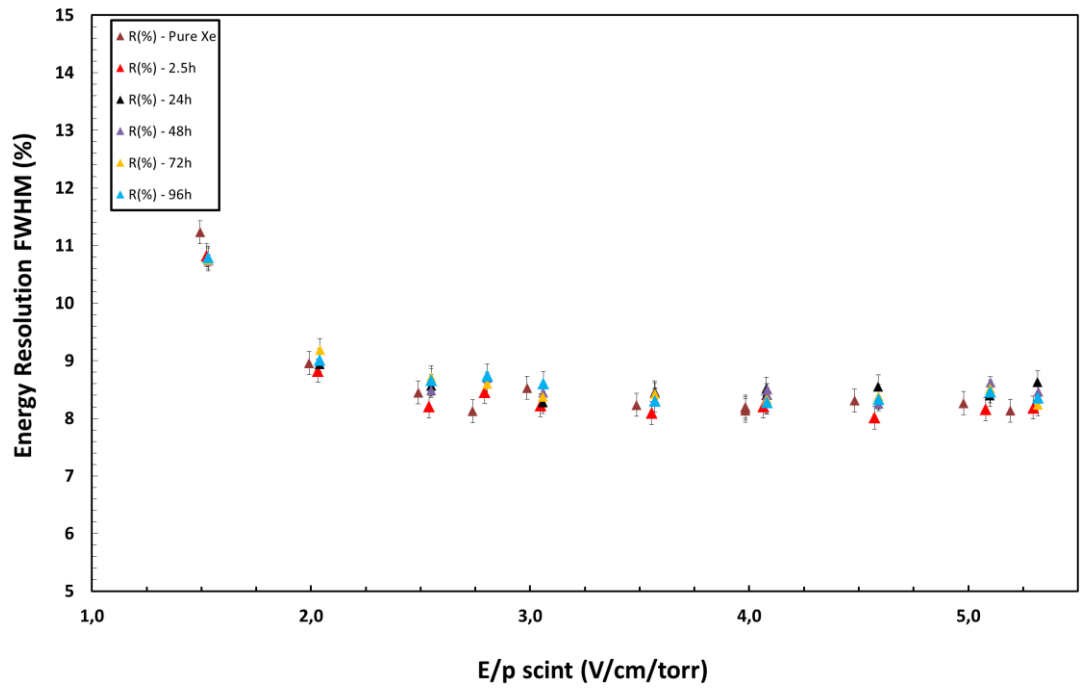

Figure 4.2. Energy resolution as a function of reduced electric field, E/p, for the mixture of 99.89% Xe+0.11% CO_2 at 80°C with a filling pressure of 750 torr, for a constant PMT bias voltage of 650 V and shaping constants of 5 μs.

Figure 4.2 presents the variation with time of the energy resolution as a function of reduced electric field, for the mixture referred to above. For pure xenon, the value of energy resolution for a reduced electric field of 4V/cm/torr is about 8.2%. With the addition of a nominal value of 0.11% of CO_2 the energy resolution deteriorated to a value of about 8.5%

4.3. Mixture of 99.67% Xe + 0.33% CO_2

Figure 4.3 and Figure 4.4 show the variation with time of the electroluminescence relative amplitude and the energy resolution as a function of reduced electric field, respectively, for a mixture of 99.67%Xe + 0.33%CO_2. The getters were still operating at a temperature of 80ºC.

The linear dependence of the electroluminescence relative amplitude remains as in the cases of pure xenon and the mixture of 99.89%Xe + 0.11%CO_2. The excitation threshold increased to a value of about 1.2V/cm/torr, higher than the one for pure xenon (1.0V/cm/torr).

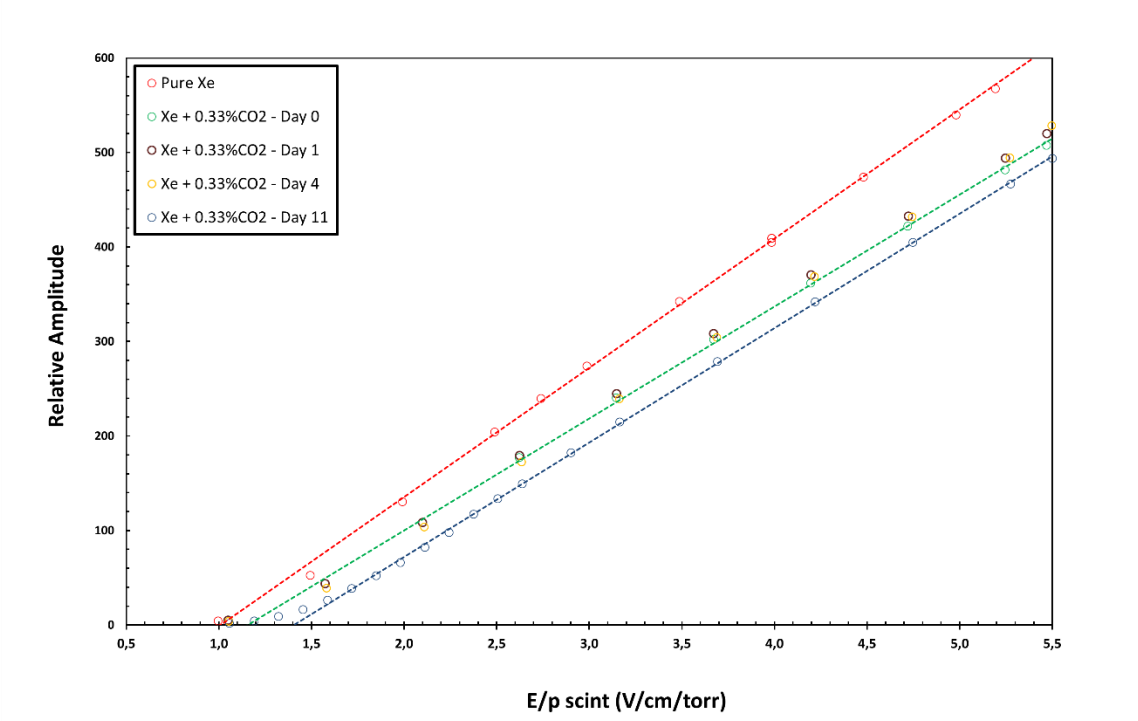

Figure 4.3. Relative amplitude as a function of reduced electric field, E/p, for the mixture of 99.67% Xe+0.33% CO_2 at 80ºC with a filling pressure of 750 torr, for a constant PMT bias voltage of 650 V and shaping constants of 5 μs.

In terms of energy resolution, the same behaviour as for pure xenon was observed, with a fast decrease with increasing E/p for low E/p values, and stabilizing for high reduced electric fields.

Generally, the energy resolution was higher than that for pure xenon and the electroluminescence relative amplitude decreased. This means that a small percentage of carbon dioxide added to xenon in the driftless GPSC absorbs the energy that primary electrons gain from the electric field through inelastic collisions by exciting rotational and vibrational modes. Therefore, a higher electric field is needed to produce the same amount of scintillation.

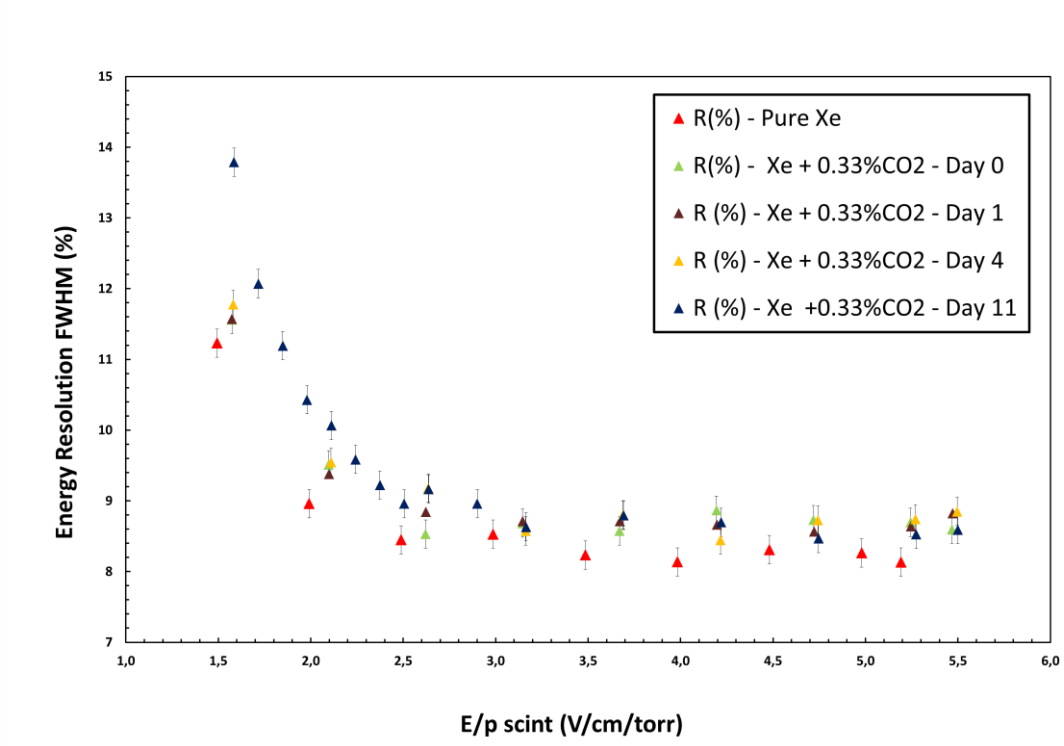

Figure 4.4. Energy resolution as a function of reduced electric field, E/p, for the mixture of 99.67% Xe+0.33% CO_2 at 80°C with a filling pressure of 750 torr, for a constant PMT bias voltage of 650 V and shaping constants of 5 μs.

As can be seen in Figure 4.3, 11 days after the second mixture was made, the excitation threshold raised abruptly. Moreover, there was deterioration of the energy resolution (Figure 4.4). Clearly, an impurity or impurities besides carbon dioxide were present in the detector.

The presence of other impurities in the detector could have been possible in two ways:

i) With the getters at a temperature of 80ºC the purification of xenon would not be efficient over time;

ii) Since the pressure of the system was about 750 torr (slightly lower than the atmospheric pressure), air from the surroundings of the system could have entered the detector, contaminating the gas mixture.

The mixture was considered not to be in proper conditions and the detector was cleaned and filled again with pure xenon.

The main detector chamber was filled with enough xenon, to have a pressure higher than the atmospheric pressure after the mixture was made.

Figure 4.5 compares the results of the amplitude and energy resolution as a function of reduced electric field for pure xenon and for the nominal mixtures of 99.89% Xe + 0.11% CO_2 and 99.67% Xe + 0.33% CO_2. The getters' operating temperature was 80ºC, the PMT bias voltage 650 V and the shaping constants 5 µs.

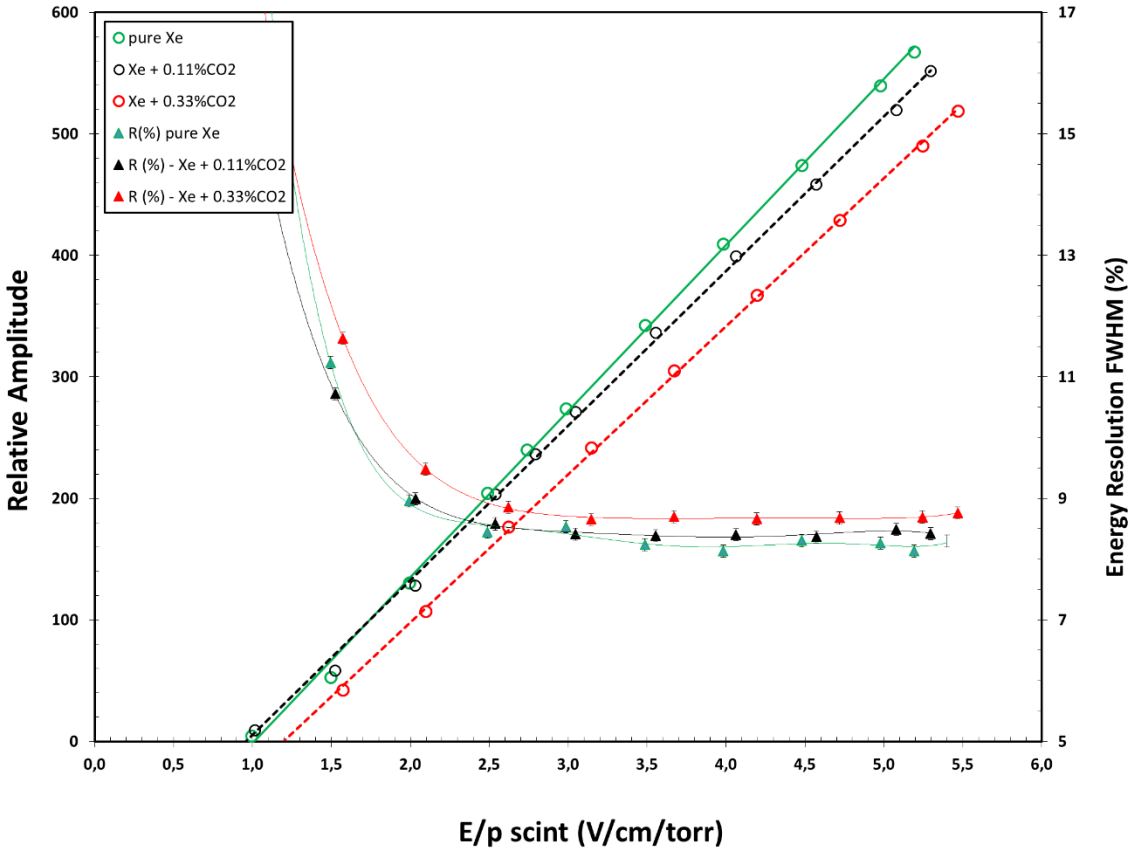

Figure 4.5. Relative amplitude and energy resolution as a function of reduced electric field, E/p, for pure xenon and for the mixtures of 99.89% Xe+0.11% CO_2 and 99.67% Xe+0.33% CO_2, for getters operating at 80ºC, a constant PMT bias voltage of 650 V and shaping constants of 5 µs.

The energy resolution still decreased with increasing reduced electric field and, at 5 V/cm/torr, was around 8.1%, 8.4% and 8.7% FWHM, for pure xenon, 99.89% Xe+0.11% CO_2 and 99.67% Xe+0.33% CO_2 nominal mixtures, respectively.

4.4. Study of Pure Xenon with Getters Operating at 80ºC

Before a new addition of carbon dioxide to xenon, a study was made to verify how long the xenon remained purified with the getters operating at 80ºC.

Figure 4.6 shows the variation with time of electroluminescence relative amplitude and energy resolution as a function of reduced electric field for pure xenon with getters operating at 80ºC.

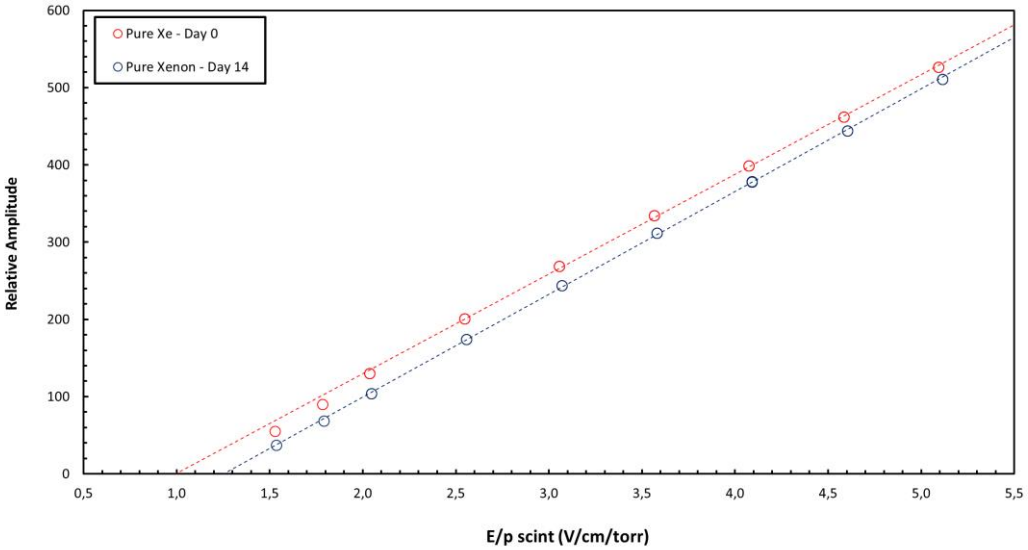

Figure 4.6. Relative amplitude as a function of reduced electric field, E/p, for pure xenon at 80ºC with a filling pressure of 763 torr, for a constant PMT bias voltage of 650 V and shaping constants of 5 μs.

As can be seen in the above figure, after 14 days the excitation threshold increased to a value of about 1.25 V/cm/torr, meaning that the xenon maintained its purity for a period of 14 days with the getters operating at 80ºC and any measurements should be made within this period of time.

Figure 4.7 shows the energy resolution as a function of reduced electric field for pure xenon in the same conditions as above. After 14 days there is a deterioration in the energy resolution. For pure xenon, the energy resolution was about 8.2% for a reduced electric field of about 4.0 V/cm/torr. In the 14th day of monitoring the energy resolution was of

about 8.4% for the same E/p. This discrepancy is due to the presence of impurities in the gas, compromising the obtained results.

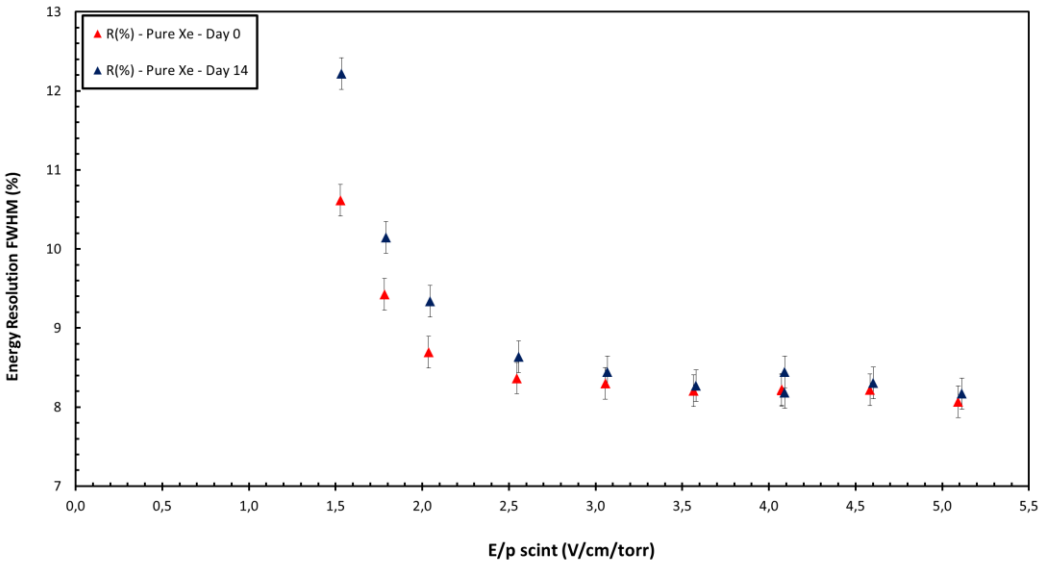

Figure 4.7. Energy resolution as a function of reduced electric field, E/p, for pure xenon at 80^{o}C with a filling pressure of 763 torr, for a constant PMT bias voltage of 650 V and shaping constants of 5 μs.

4.5. Electroluminescence Yield

Figure 4.8 presents the reduced EL yield, Y/N, i.e. the EL yield divided by the density of the gas, as a function of reduced electric field, E/N, in the scintillation region of the driftless GPSC. Experimental results from other authors and results from Monte Carlo simulation [47] are included for comparison.

The absolute values presented in this work were obtained by normalizing the relative values measured for pure xenon to the absolute values of Monteiro et al. [48].

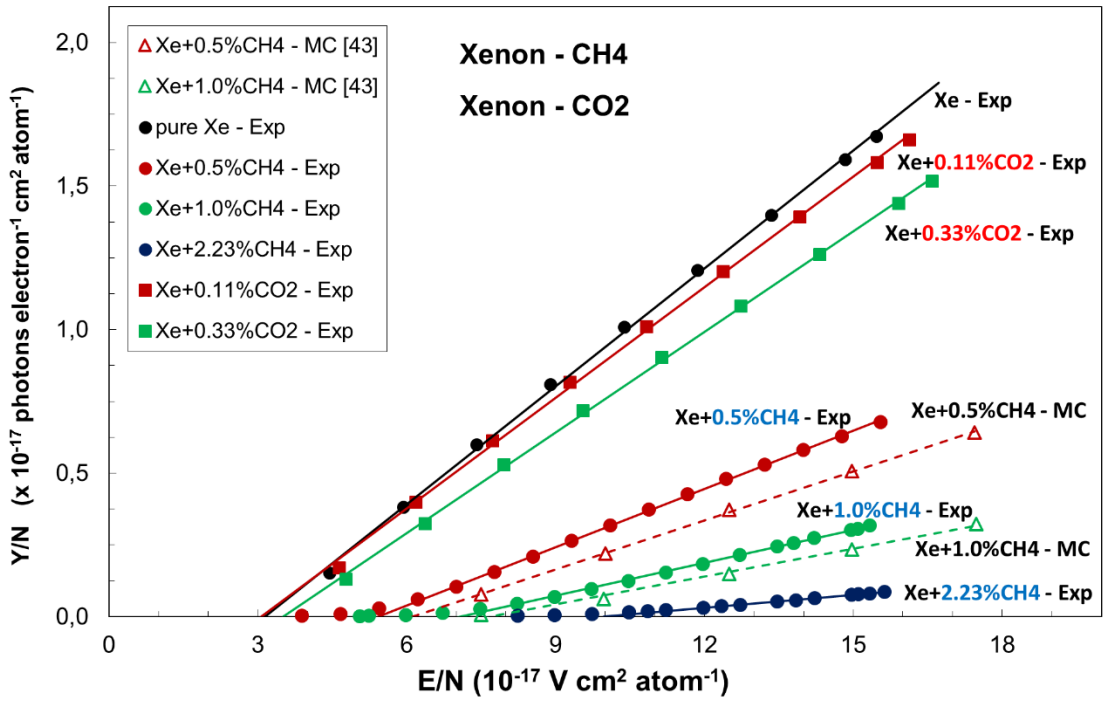

Figure 4.8. Xenon reduced electroluminescence yield as a function of E/N for our studies, as well as for Monte Carlo data in the literature.

As expected, the addition of molecular gases to pure xenon reduces the electroluminescence yield of the gas mixture, decreasing with increasing molecular additive concentration.

The primary electrons drift across the scintillation region undergoing a very large number of elastic collisions with the gas atoms/molecules. Since the mass difference between electron and atoms is very high, the amount of energy lost in one elastic collision is negligible. Thus, the energy transfer from the electric field to the electrons is very efficient. When the electrons acquire enough energy to excite the xenon atoms an elastic

collision may occur leaving the atom in an excited state. In a collision between the electron and a polyatomic molecule, the electron energy may be lost to rotational and vibrational states, without the emission of electroluminescence, resulting in a reduced yield. Since the number of inelastic collisions between two elastic collisions is higher than 10^4 [46], this effect becomes noticeable for molecular concentrations as low as few tenths of percent for CH_4 and CO_2.

The addition of CO_2 seems to have less impact on the electroluminescence yield and on the electroluminescence threshold than CH_4, which is a more complex molecule with more vibrational modes causing electrons to have higher energy losses along their path in the scintillation region.

Compared to pure xenon, the EL yield decreases to about 95% and 80% for 0.11%, and 0.33% of CO_2, respectively, for E/p between 1.5 and 2.25 V cm^{-1} $torr^{-1}$, a typical reduced electric field used in the NEXT-DEMO TPC, while for CH_4 this decrease is to about 30%, 10% and less than 3% for 0.5%, 1.0% and 2.2% CH_4, respectively. The amplification parameters (the slope of the linear fits to the scintillation yield) and respective gas electroluminescence thresholds for the above mixtures are presented in Table 1.

Gas/Gas Mixture	***Amplification Parameter (photons/kV)***	***Electroluminescence Threshold (kV/cm/bar)***
Pure Xenon	137	1.0
Xe+0.11%CO_2	128	1.0
Xe+0.33%CO_2	117	1.2
Xe+0.5%CH_4	68	1.8
Xe+1.0%CH_4	38	2.3
Xe+2.2%CH_4	15	3.3

Table 1. Amplification parameters and electroluminescence thresholds for pure xenon and for the different gas mixtures.

Figure 4.9 presents the electroluminescent yield experimental results (solid circles) for pure xenon and for the mixtures of 99.89% Xe+0.11% CO_2 and 99.67% Xe+0.33% CO_2, along with the Monte Carlo simulations (empty circles) for the same mixtures, and for pure xenon along with the mixtures of 99.9%Xe + 0.01%CO_2 and 99.95Xe + 0.05%CO_2.

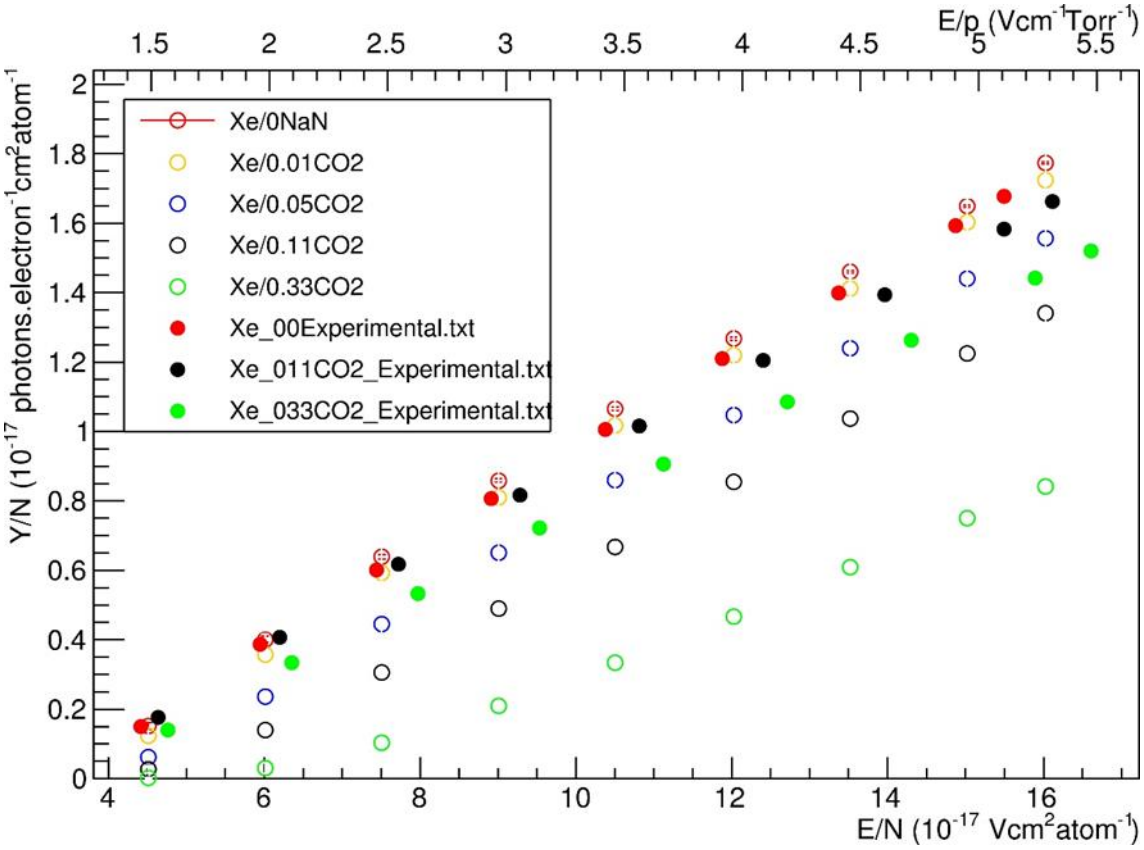

Figure 4.9. Xenon reduced electroluminescence yield as a function of E/N for our studies, as well as for Monte Carlo data. (C.D.R. Azevedo, private communication)

As can be seen, the experimental results obtained for the referred mixtures and the simulation results are far from matching. For example, the electroluminescence yield for the experimental mixture of 0.11% CO_2 is higher than the simulation result of 0.05% CO_2, and is very close to the 0.01% CO_2 result. This could mean that the getters operating at 80ºC were absorbing CO_2. In addition, CO_2 may be attached to the detector walls, leading to a mismatch between the nominal concentration of CO_2 added to xenon and the actual CO_2 content of the mixture. This was already noticed for the Xe-CH_4 mixtures, where the experimental values for the EL Yield approach simulation results as the CH_4 nominal concentration increases, being already similar for 2.0% CH_4, meaning that for such

amount of CH_4 the number of molecules that migrate from the gas volume to the detector surfaces is already negligible.

From Figure 4.9 can be noticed that the nominal value of 0.33% may correspond to an actual CO_2 concentration somewhat above 0.05%. Therefore, the next step taken in this work was to fill the detector with a mixture of 99.5% Xe+0.5% CO_2.

4.6. Mixture of 99.5% Xe+0.5% CO_2

In this section the effect of the 99.5% Xe+0.5% CO_2 mixture was studied. Figure 4.10 shows the variation of the electroluminescence relative amplitude on the reduced electric field with time, when 0.5% of CO_2 was added to xenon and the getters were operating at a temperature of 80ºC.

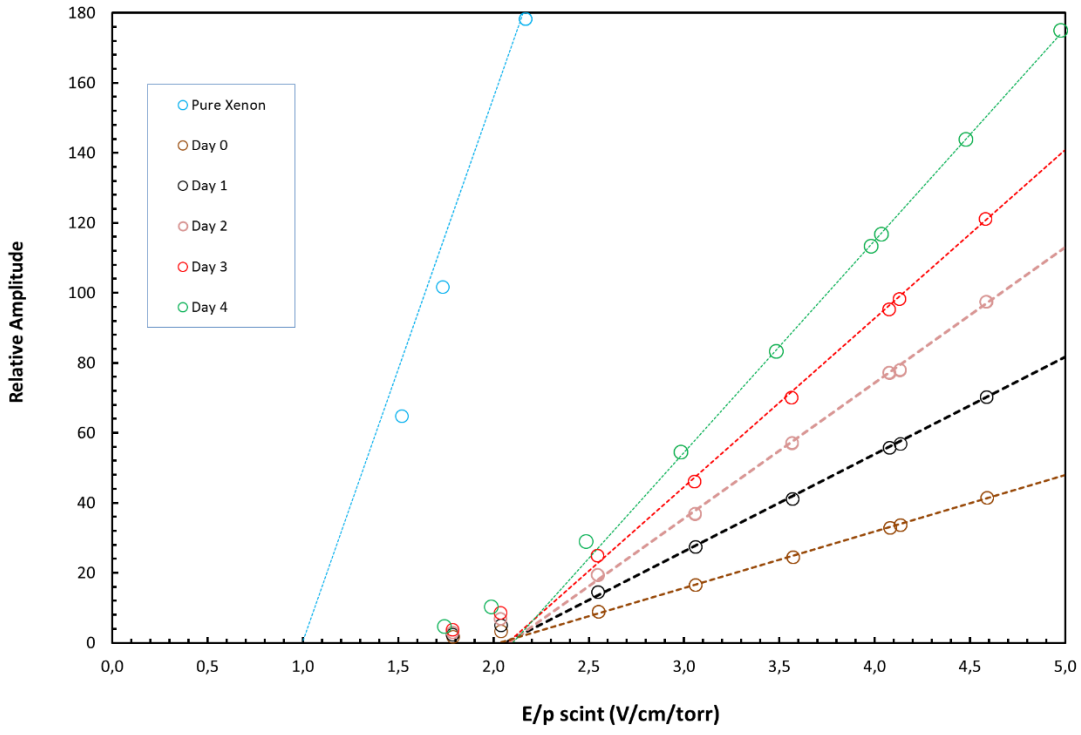

Figure 4.10. Relative amplitude as a function of reduced electric field, E/p, for pure xenon and for the mixture of 99.5% Xe+0.5% CO_2, for getters operating at 80ºC, a constant PMT bias voltage of 650 V and shaping constants of 5 μs.

Comparing with the results obtained for pure xenon, the addition of this percentage of CO_2 had a drastic impact on the electroluminescence relative amplitude, which decreased abruptly. However, this relative amplitude increased over time.

Figure 4.11 shows a detailed view of the electroluminescence relative amplitude variation with time as a function of reduced electric field, to better understand the behaviour of the excitation threshold. This threshold increased to a value between 2.0V/cm/torr and 2.1V/cm/torr and was within this range during the 4 days that the mixture was monitored.

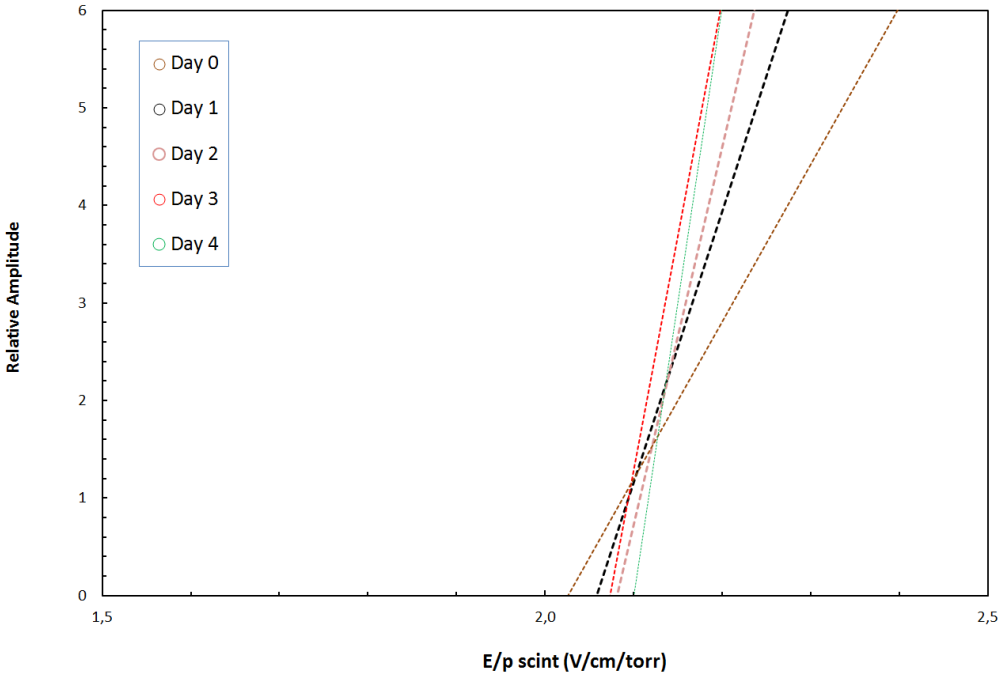

Figure 4.11. Relative amplitude as a function of reduced electric field, E/p, for pure xenon and for the mixture of 99.5% Xe+0.5% CO_2, for getters operating at 80ºC, a constant PMT bias voltage of 650 V and shaping constants of 5 μs.

Figure 4.12 shows the variation of the energy resolution as a function of reduced electric field with time for the 99.5%Xe + 0.5%CO_2 mixture.

With this mixture the energy resolution deteriorated, increasing from a value of about 8% for pure xenon and a reduced electric field of 5V/cm/torr, to a value of about 13% for the same reduced electric field, hours after the mixture was made. As time passed, the energy resolution improved to a value of about 9%.

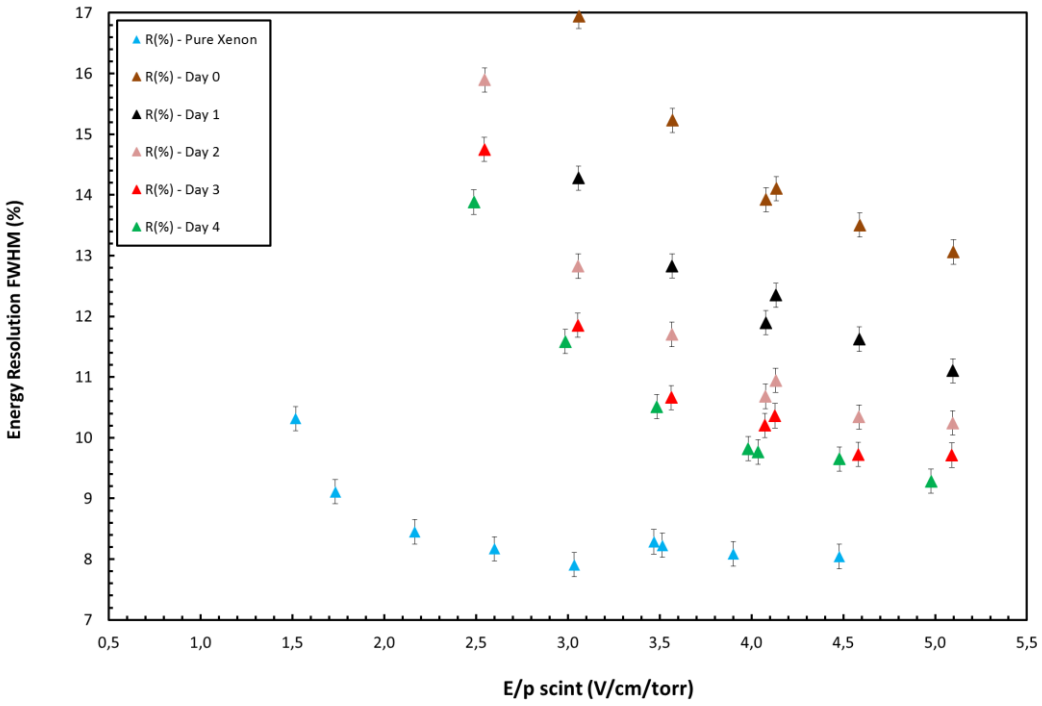

Figure 4.12. Energy resolution as a function of reduced electric field, E/p, for pure xenon and for the mixture of 99.5% Xe+0.5% CO_2, for getters operating at 80°C, a constant PMT bias voltage of 650 V and shaping constants of 5 μs.

The fact that the electroluminescence relative amplitude and the energy resolution did not stabilize with time suggests that the getters could be absorbing CO_2. However, there was also the odd fact that the excitation threshold was not approaching that of pure xenon, rather had stabilized around the 2.1V/cm/torr. There could be another effect, namely the presence of another species due to the getters operation; as CO_2 passes through the getters, e.g. there could be dissociation of CO_2 into CO+O.

An interesting study could be to do this last mixture without using getters' purification. For that, one needs to know how long the mixture can be studied before the xenon is not pure anymore and/or to learn how the detector performance degrades without the purifying action of the getters.

4.7. Study of Xenon without getters purification

In this section was performed the study of the response with time of the pure xenon when the getters are not purifying the gas. For that, valves T_2 and T_3 were closed.

The main purpose of this procedure is to know the rate at which the electroluminescence light produced in xenon will decrease with time and how much the energy resolution deteriorates.

Figure 4.13 shows the variation of the electroluminescence relative amplitude as a function of time for pure xenon and without getter operation, for a constant reduced electric field of 3.5 V/cm/torr.

The relative amplitude decreases linearly with time, losing around 3 channels every ten minutes. This means that, when getter system is not operating, the xenon becomes more and more impure at a constant rate.

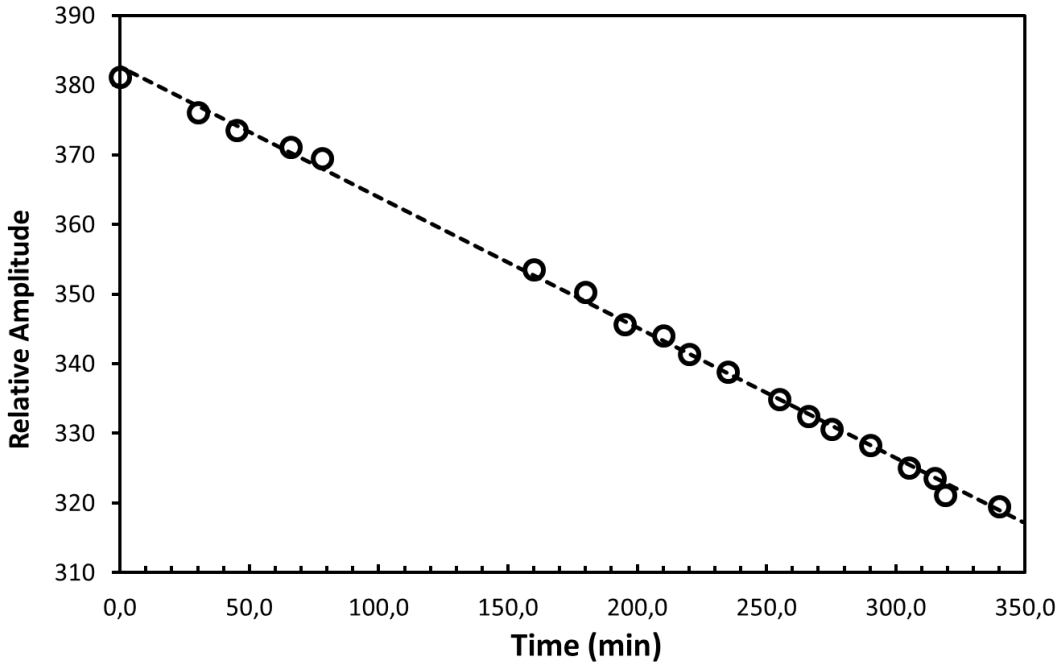

Figure 4.13. Relative amplitude as a function of time, for pure xenon without the operation of the getter purifying system, for a constant reduced electric field of 3.5 V/cm/torr, a constant PMT bias voltage of 650 V and shaping constants of 5 μs.

In Figure 4.14 the variation of the energy resolution is represented as a function of time. During the 5 hours that the measurements were taken, the energy resolution increased from a value of about 7.9% to a value of about 9.0%.

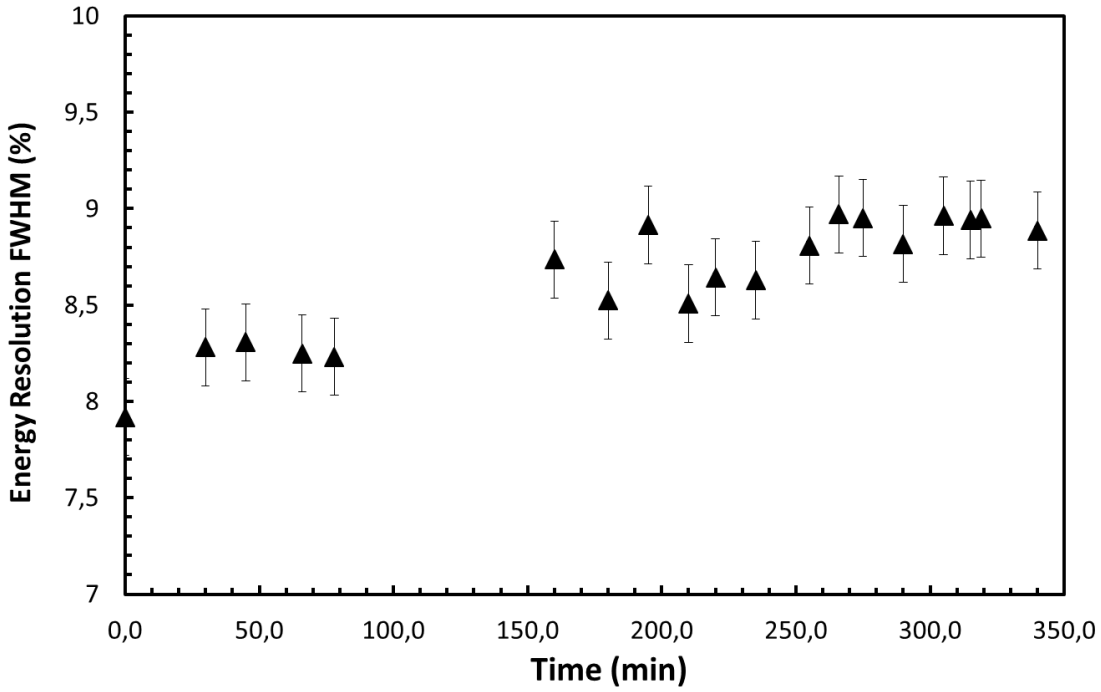

Figure 4.14. Energy resolution as a function of time, for pure xenon without the getters purifying system, a constant reduce electric field of 3.5V/cm/torr, a constant PMT bias voltage of 650 V and shaping constants of 5 μs.

4.8. Study of the mixture of 99.5%Xe+0.5%CO_2 without getters purification

After the previous study on xenon without getter operation, valves T_2 and T_3 were opened and the getters' temperature was raised to 180ºC to purify the xenon. The performance of the detector was tested and, when the xenon was purified, CO_2 was added to the detector chamber following previous procedures. At the same time valves T_2 and T_3 were closed so that the getters would not affect the CO_2.

The time that this percentage of CO_2 and the xenon took to fully mix is not known and, hence, the data were taken in short periods of time of about 30 minutes.

Figure 4.15 shows the variation with time of the electroluminescence relative amplitude as a function of reduced electric field for the mixture of 99.5% Xe+0.5% CO_2. The same figure shows also the curve of pure xenon for comparison with the results of the referred mixture.

In the first half hour after the mixture was made, an abrupt decrease of EL occurred, as can be seen by the decrease in the electroluminescence relative amplitude. This decrease continued to occur with time, and is due to the CO_2 addition as well as to the fact that the xenon was getting impurities from the system, since the getters were not operating. These measurements were taken for about four hours and during this time the relative amplitude did not stabilize.

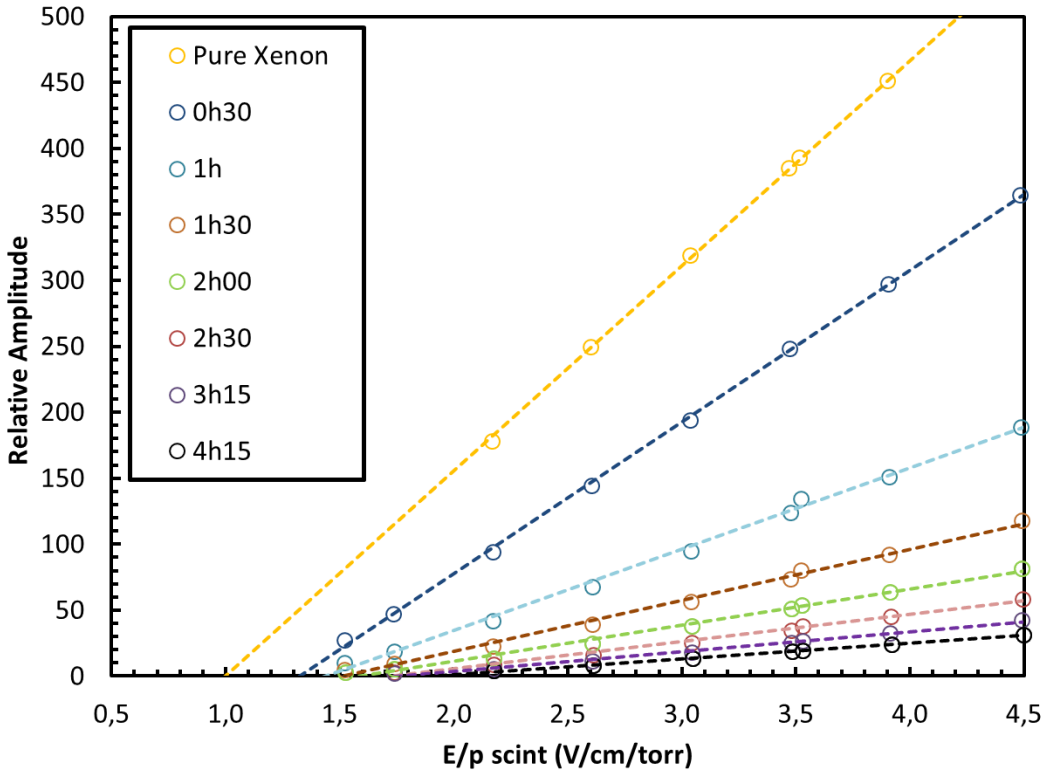

Figure 4.15. Relative amplitude as a function of reduced electric field, E/p, for pure xenon and for the mixture of 99.5% Xe+0.5% CO_2, without the getters purifying system, for a constant PMT bias voltage of 650 V and shaping constants of 5 μs.

Figure 4.16 shows a zoom-in on the electroluminescence relative amplitude variation with time as a function of reduced electric field, to better visualize the behaviour of the excitation threshold. It increased gradually with time from a value of 1V/cm/torr to a value of about 1,97V/cm/torr.

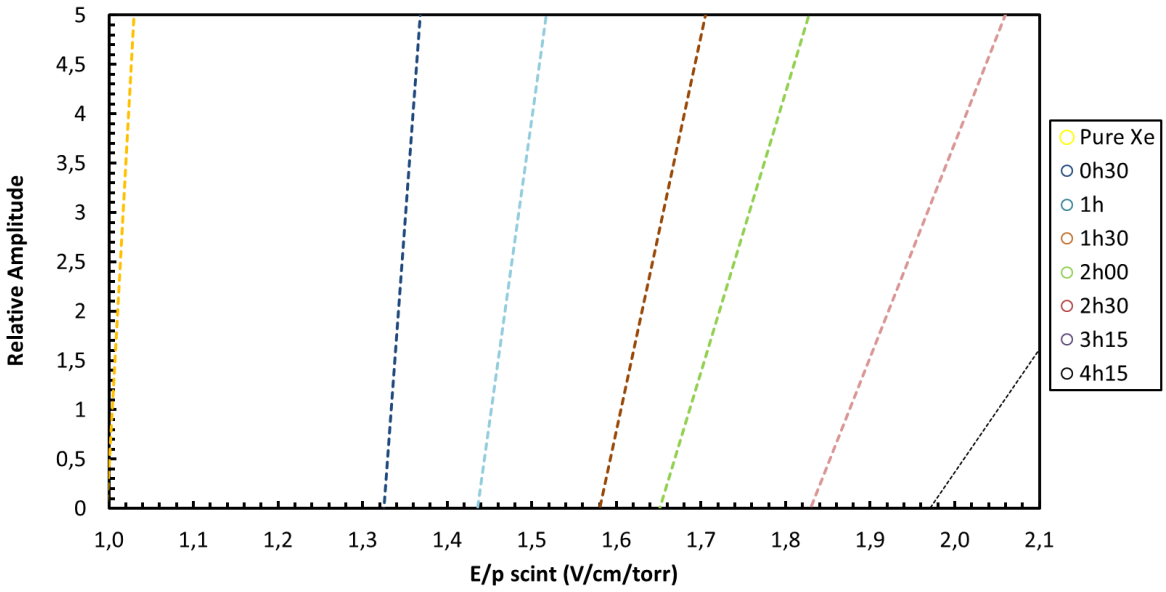

Figure 4.16. Relative amplitude as a function of reduced electric field, E/p, for pure xenon and for the mixture of 99.5% Xe+0.5% CO_2, without the getters purifying system, for a constant PMT bias voltage of 650 V and shaping constants of 5 μs.

Figure 4.17 presents the variation of the electroluminescence relative amplitude with time, for a constant reduced electric field of 3.5 V/cm/torr, for pure xenon and for the mixture of 99.5%Xe+0.5%CO_2, without getters operation. The deterioration of EL production is faster for the Xe-CO_2 mixture than for pure xenon. The CO_2 could induce the presence of water molecules, or other molecular species as carbon monoxide. In this way, the collision of the electrons with these impurities reduces drastically the production of EL.

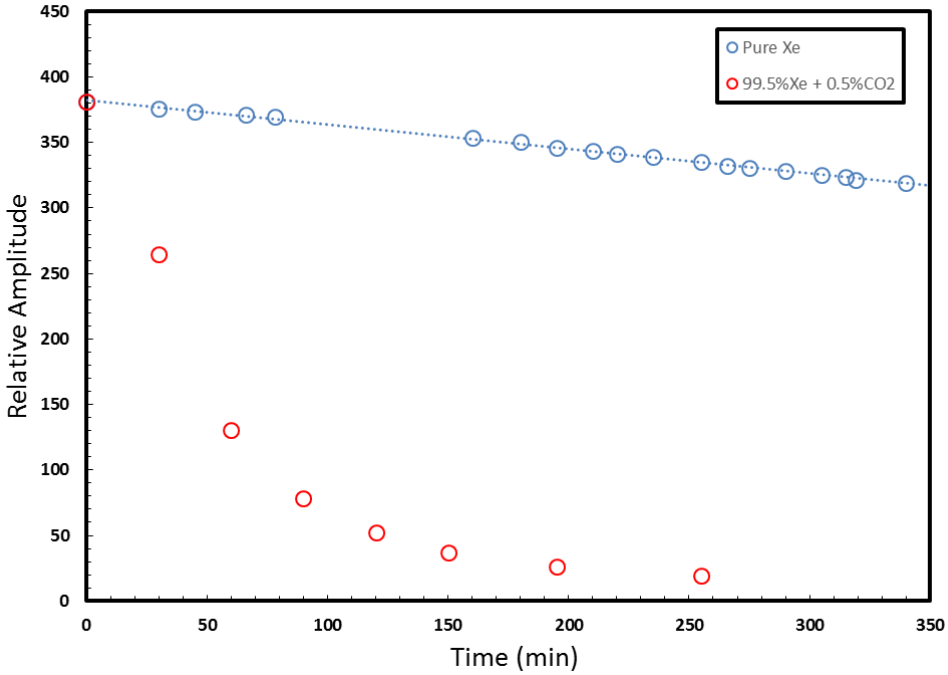

Figure 4.17. Variation of the relative amplitude with time, for a reduced electric field, E/p, of 3.5 V/cm/torr for pure xenon and for the mixture of 99.5% Xe+0.5% CO_2, without the getters purifying system, for a constant PMT bias voltage of 650 V and shaping constants of 5 μs.

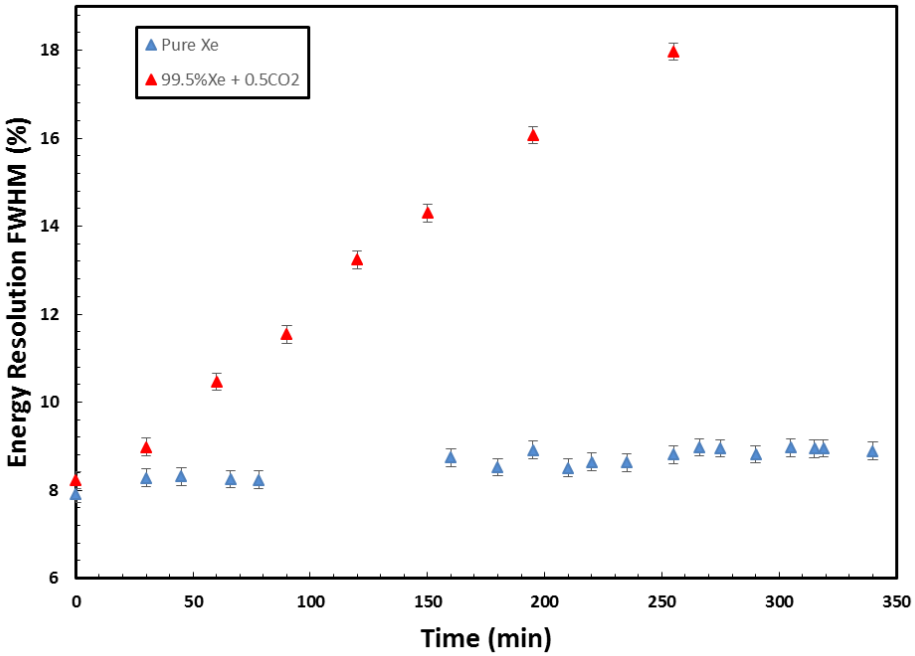

Figure 4.18. Variation of the energy resolution with time, for a reduced electric field, E/p, of 3.5 V/cm/torr for pure xenon and for the mixture of 99.5% Xe+0.5% CO_2, without the getters purifying system, for a constant PMT bias voltage of 650 V and shaping constants of 5 μs.

Figure 4.19 shows the variation with time of the energy resolution as a function of reduced electric field, for the mixture of 99.5%Xe + 0.5%CO_2. From the figure it is notorious that the energy resolution was gradually deteriorating. For pure xenon, the energy resolution was around 8% and 4 hours and 15 minutes after the mixture was made, energy resolution was around 17% for a reduced electric field of about 4.5V/cm/torr.

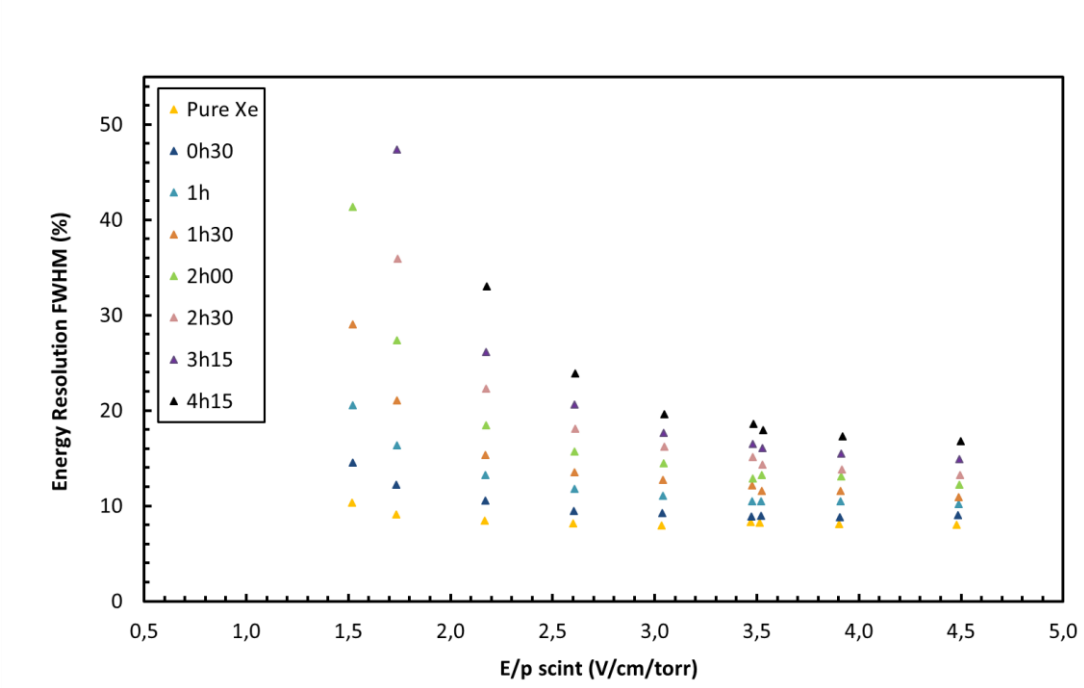

Figure 4.19. Energy resolution as a function of reduced electric field, E/p, for pure xenon and for the mixture of 99.5% Xe+0.5% CO_2, without the getters purifying system, for a constant PMT bias voltage of 650 V and shaping constants of 5 μs.

After this study without getters was made, valves T_2 and T_3 were opened and the variations of electroluminescence relative amplitude, the excitation threshold and the energy resolution were monitored.

Figure 4.20 shows the variation with time of the electroluminescence relative amplitude of the mixture of 99.5%Xe+0.5%CO_2 as a function of the reduced electric field, E/p. The effect of the getters is clear, as can be verified by the abrupt increase in EL.

Figure 4.21 shows a zoom-in on Figure 4.20, in order to verify the behaviour of the scintillation threshold, which is 1.0V/cm/torr for pure xenon. It starts at a value of about 1.95V/cm/torr and during the subsequent days it remains within the range of 1.8 and 1.84V/cm/torr.

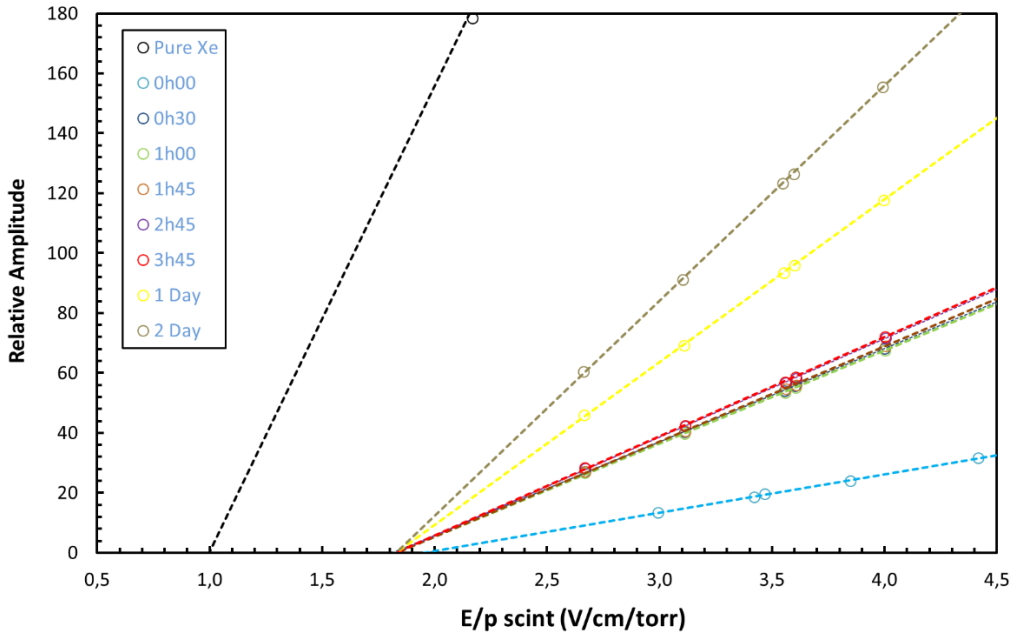

Figure 4.20. Relative amplitude as a function of reduced electric field, E/p, for pure xenon and for the mixture of 99.5% Xe+0.5% CO_2, for getters operating at 80°C, for a constant PMT bias voltage of 650 V and shaping constants of 5 μs.

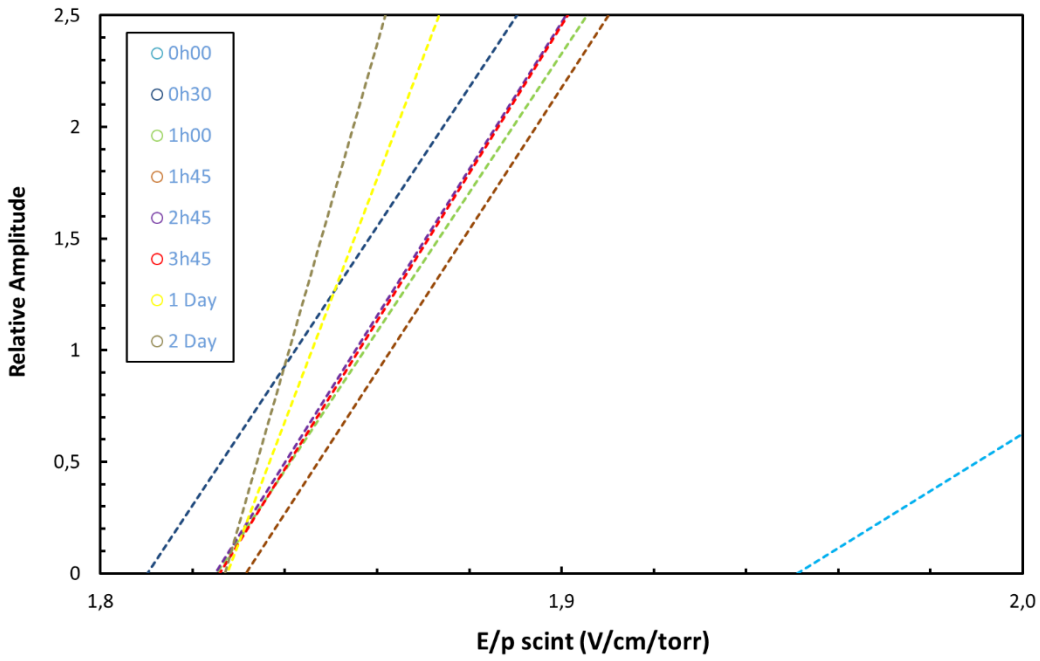

Figure 4.21. Relative amplitude as a function of reduced electric field, E/p, for pure xenon and for the mixture of 99.5% Xe+0.5% CO_2, for getters operating at 80°C, for a constant PMT bias voltage of 650 V and shaping constants of 5 μs.

Figure 4.22 shows the evolution with time of the energy resolution, as a function of reduced electric field, E/p. In two days of operation the energy resolution improved considerably, approaching that of pure xenon in the region of high reduced electric fields.

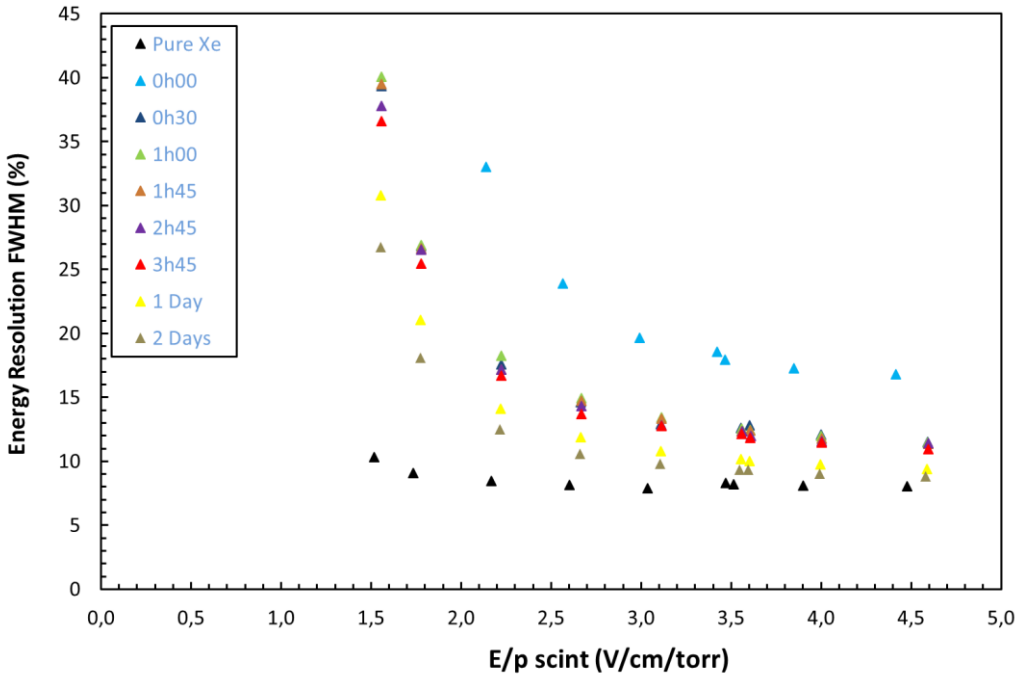

Figure 4.22. Energy resolution as a function of reduced electric field, E/p, for pure xenon and for the mixture of 99.5% Xe+0.5% CO_2, for getters operating at 80^{o}C, for a constant PMT bias voltage of 650 V and shaping constants of 5 μs.

The experimental results show that the getters do absorb CO_2 even for temperatures as low as 80ºC. We note that this temperature is not enough to guarantee total purification of the gas inside the detector, as clearly demonstrated in the studies presented in section 4.4. Nevertheless, for a much cleaner vessel and gas system, this temperature may be effective, but the operation at such low temperatures may be a risk that should not be taken during NEXT-NEW operation.

For a period of a couple hours the electroluminescence relative amplitude, the energy resolution and the scintillation threshold did not fluctuate significantly for the mixture of 99.5%Xe+0.5%CO_2. An interesting study would be to compare again the experimental data obtained with the Monte Carlo simulations for the scintillation yields.

Included in the Figure 4.23 are the data from the first mixture of 99.5%Xe +0.5%CO_2, which was taken 2.5 hours after the gases were mixed.

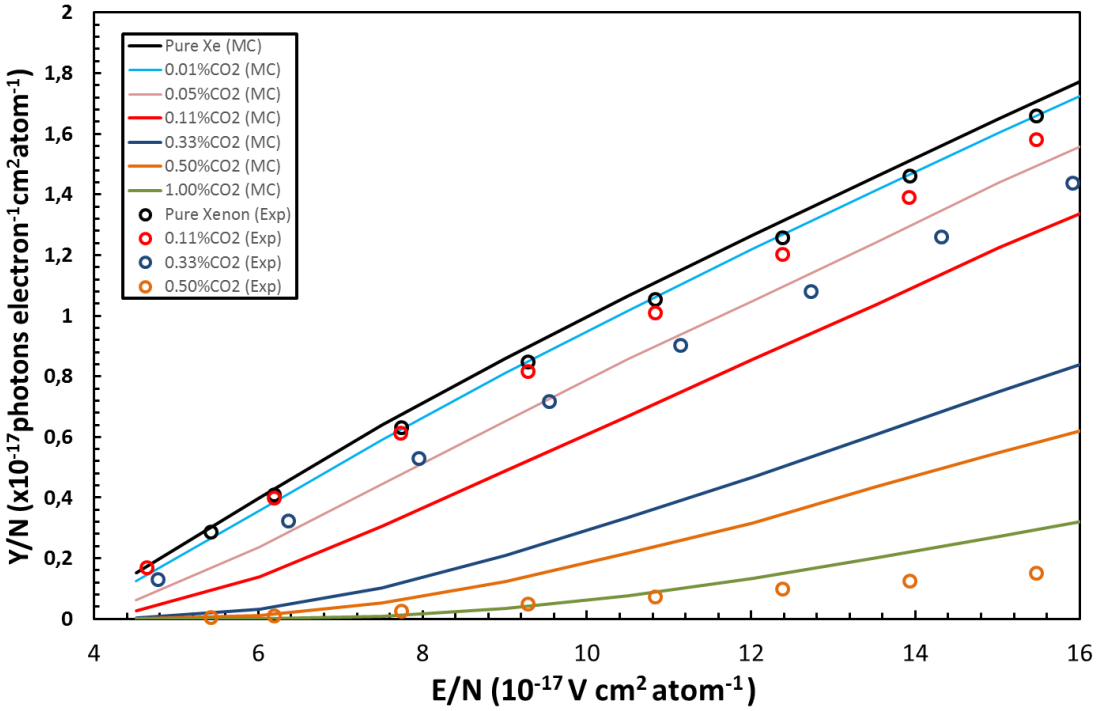

Figure 4.23. Xenon reduced electroluminescence yield as a function of E/N for our studies, as well as for Monte Carlo data, including the experimental data for the mixture of 99.5%Xe+0.50%CO_2.

The electroluminescence yield for the experimental data of the mixture of 99.5%Xe+0.5%CO_2 is closer to the results of the Monte Carlo simulation for 1%CO_2 than the one obtained for 0.5%CO_2. It is important to note that these simulation results did not have into consideration the effects of VUV quenching. Comparing the experimental results obtained for 0.11% and 0.33%CO_2 with the result obtained for 0.5%CO_2 one can observe that this effect is very severe for the latter. And, if this is true for our detector that has a scintillation thickness of 2.5cm, it would be even worse for the NEXT detector.

It is expected that, when the VUV quenching effect is considered in the simulations, the results will approach that of experimental data of 0.5%CO_2 and will deviate even more from the results obtained for the experimental data of 0.11% and 0.33%CO_2.

4.9. Energy Resolution

The statistical fluctuations associated to the electroluminescence production and readout are an important parameter to be considered, since this is a major requirement for background reduction in double beta decay detectors. Figure 4.24 depicts the energy resolution (FWHM) obtained in the driftless GPSC for the different gas mixtures.

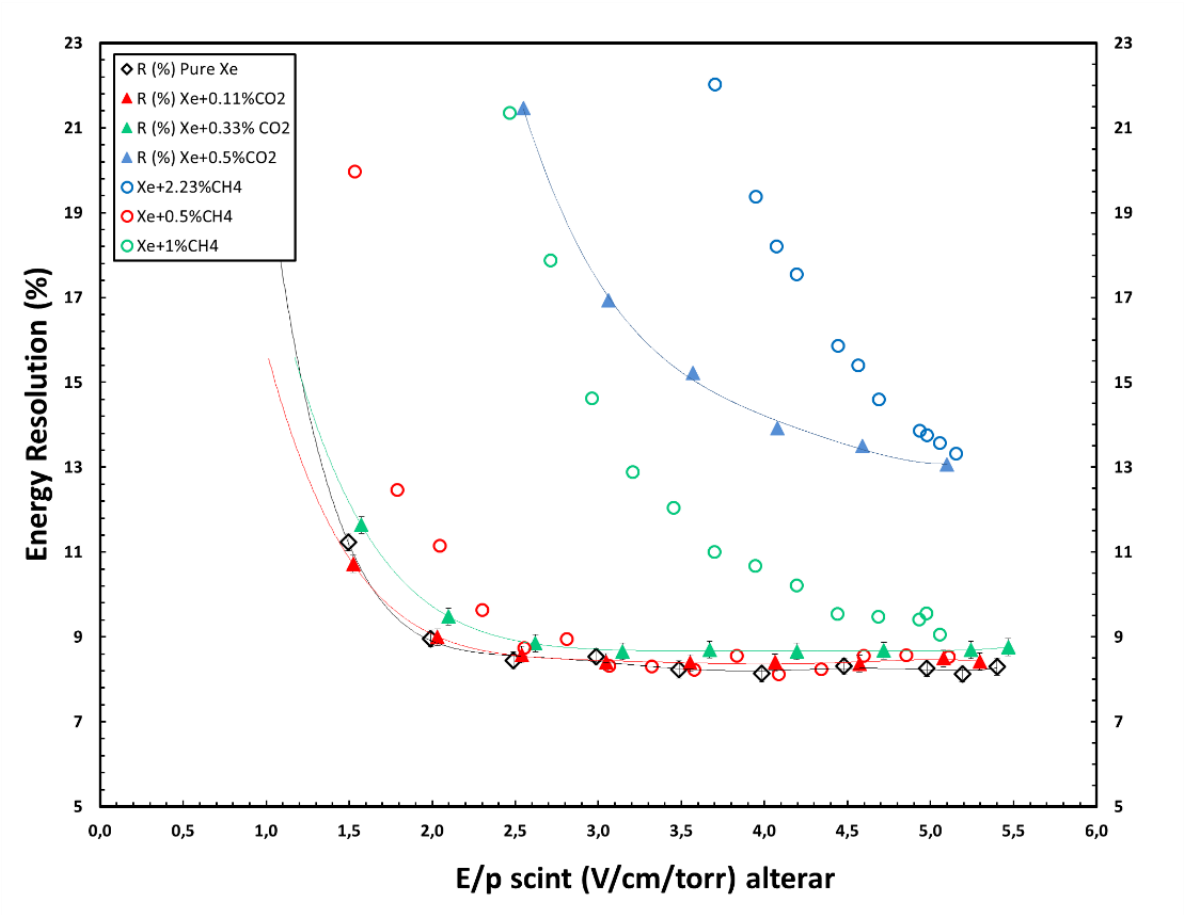

Figure 4.24. Energy resolution (FWHM) as a function of reduced electric field in the scintillation region, for pure xenon and for the Xe-CH_4 and Xe-CO_2 mixtures studied in this work. The lines serve only to guide the eye.

As seen in Figure 4.24, the higher the fraction of molecular additive, the higher the energy resolution. For instance, for an E/p value of about 2.7 V/cm/torr, the energy resolution has values of about 8.6% and 9.0% for CO_2 concentration of 0.11%, and 0.33%, respectively, at an E/p value of about 2.7 V/cm/torr. However, operating at higher reduced electric fields in the scintillation region improves the energy resolution to values

close to those obtained for pure xenon. For Xe+1%CH_4 much higher electric field values would be needed in order to achieve such energy resolutions, while with Xe+2%CH_4 it is impossible to achieve good energy resolutions, as denoted in Figure 4.24. However, we note that the nominal value for 0.33% of CO_2 corresponds, in fact, to a ~0.06% of CO_2 concentration in the gas mixture. An actual concentration of CO_2 between 0.2 – 0.25% is needed to optimize the electron diffusion parameters of the Xe-CO_2 mixtures.

Nevertheless, our studies with the nominal value of 0.5% CO_2 have showed that CO_2 mixtures do not guarantee a stable operation, which is a serious drawback to their use in NEXT.

As N_e is proportional to the pulse amplitude, a plot of R^2 as a function of the inverse of the relative amplitude, varying the reduced electric field in the scintillation region, will present a linear trend, from which the detector limit resolution can be obtained by extrapolating the trendline to infinite light yield.

$$R(FWHM)\% = 2.355\sqrt{\frac{FW}{E_x} + \frac{2}{N_e}} \tag{35}$$

Figure 4.25 depicts the R^2 dependence on A^{-1} for the present GPSC and for the different gas mixtures. A linear trend is observed for a certain range of amplitudes. The deviation from this trend is due to different processes occurring in the detector as the reduced electric field in the scintillation region changes. For instance, the detector energy resolution degrades for high reduced electric fields due to the additional electronic fluctuations introduced by instabilities in the electric insulation and/or to the additional statistical fluctuations introduced by electron multiplication, for electric field values above the gas ionization threshold. On the other hand, for low values of the reduced electric field, the energy resolution degradation is faster than predicted by Eq.(35) due to the poorer signal-to-noise ratio and higher diffusion of primary electrons, which introduce additional fluctuations in the measured pulse amplitudes.

(a)

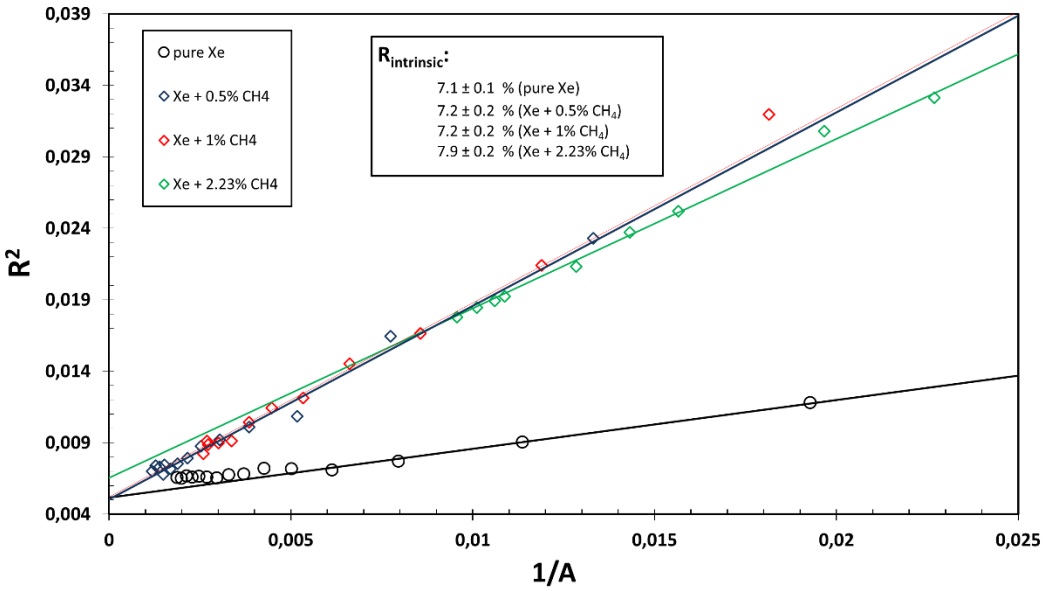

(b)

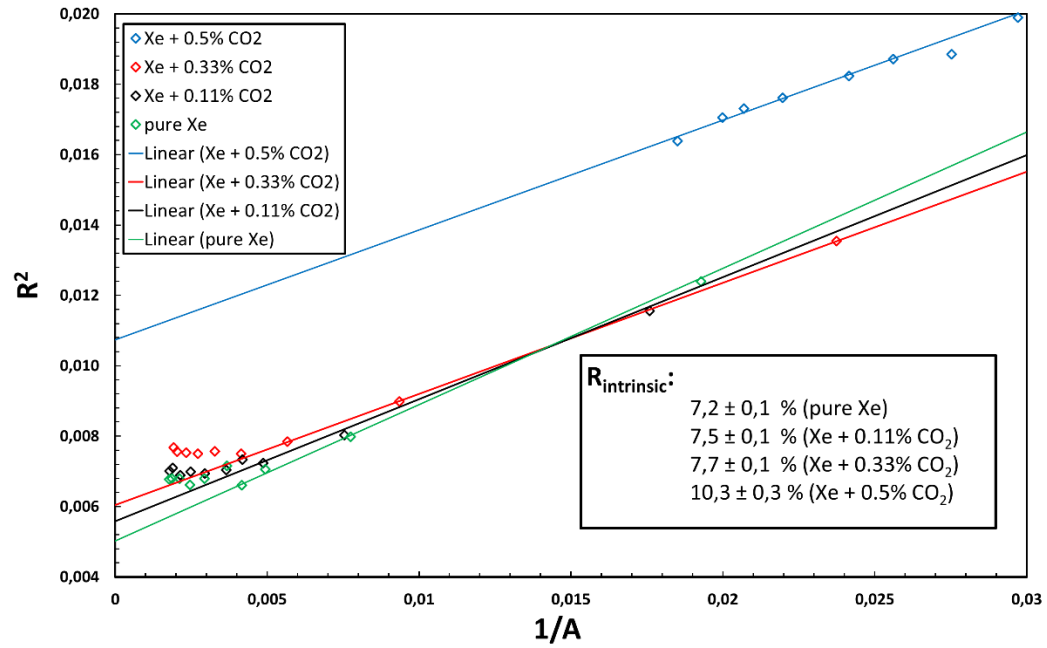

Figure 4.25. Dependence of R^2 on A^{-1} for the GPSC used in this work, for the different $Xe+CH_4$ mixtures (a) and different $Xe+CO_2$ mixtures (b). As expected, a linear trend is observed for a certain range of amplitudes.

Table 2 presents the experimental values for the intrinsic energy resolution obtained for the different mixtures. These values present an upper limit, since the experimental values obtained for the GPSC energy resolution include additional contributions inherent to the present experimental setup, experimental conditions and gas purity. The data suggests that Xe-CO_2 mixtures lead to worse energy resolution, which may be tolerable for CO_2 true concentrations around or below 0.1%, but may be too high for concentrations around or above 0.2%.

Gas/Gas Mixture	Intrinsic Energy Resolution FWHM(%)
Pure Xe	7.1 ± 0.2
Xe + 0.11%CO_2	7.3 ± 0.2
Xe + 0.33%CO_2	7.7 ± 0.2
Xe + 0.50%CO_2	10.3 ± 0.3
Xe + 0.50%CH_4	7.1 ± 0.2
Xe + 1.00%CH_4	7.3 ± 0.2
Xe + 2.20%CH_4	8.1 ± 0.2

Table 2. Values of the intrinsic energy resolution, FWHM, for the different gas mixtures.

4.10. Electron Drift Velocity

Another study carried out in this work was the measurement of the drift velocity of electrons in pure xenon and in the different mixtures of Xe-CO_2..

The drift velocity of an electron cloud is defined as [49]:

$$w = \frac{d}{T} \tag{36}$$

where d is the distance that the electron cloud travels in the detector and T is the drift time. In [50]**,** T is defined as the time that the centre of the electron cloud takes to travel from the point where it was created to the point where it reaches the anode, and can be written as:

$$T = T_t - \frac{1}{2}T_f \tag{37}$$

where T_t is the total duration of the electric signal and T_f is the fall time. These two parameters are measured through the use of an oscilloscope (Teledyne Lecroy – Wave Runner 610Zi 1GHz 20GS/s).

With this oscilloscope we can obtain a histogram of the total pulse duration and a histogram of the fall time of the electric pulses. The values of the total and the fall time were obtained considering the mode of the histogram of 1000 pulses as the most probable value. The fall time was measured from 95% to 5% of the pulse height.

Figure 4.26 shows one image of results obtained with the oscilloscope used in our work. This figure presents the output signal and the typical histograms of the fall time (cyan) and the full time (yellow) for 1000 pulses.

Figure 4.26. Signal output and histograms of the fall time (cyan) and full time (yellow) obtained with a driftless GPSC, for the mixture of 99.89%Xe+0.11%CO_2, for a reduced electric field, E/p, of 2.55V/cm/torr.

Figure 4.27 shows the drift velocity of electrons as a function of the reduced electric field, E/p, for pure xenon and for the different mixtures of Xe-CO_2.

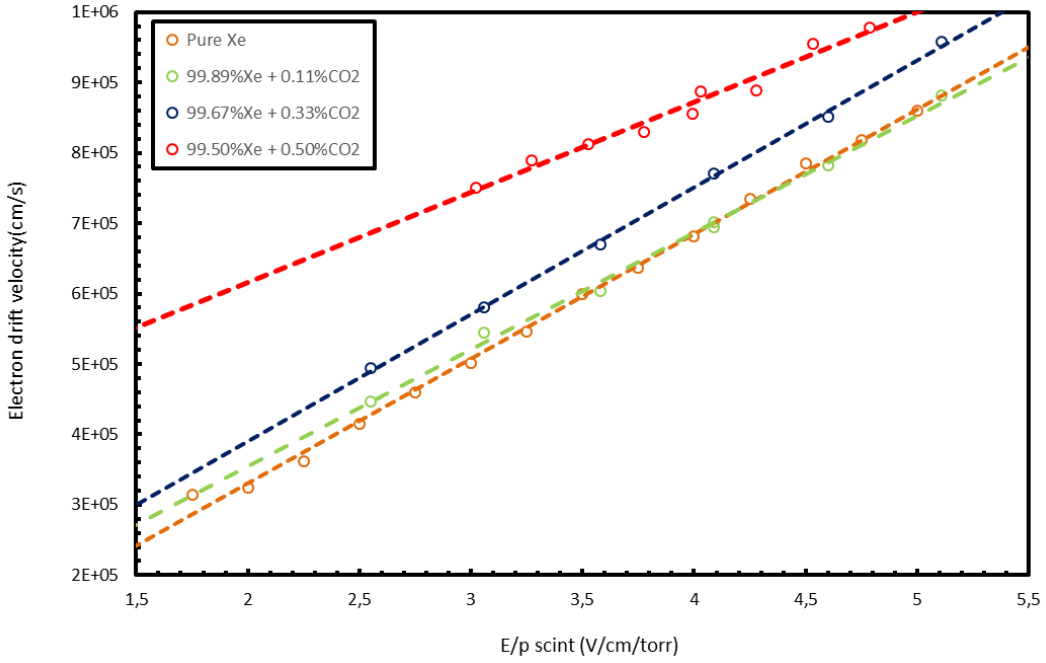

Figure 4.27. Electron drift velocity as a function of reduced electric field, E/p, for pure xenon and for the different Xe-CO2 mixtures, for getters operating at 80^{o}C, a constant PMT bias voltage of 800 V and shaping constants of 50 ns.

As can be seen, compared with pure xenon, the electron drift velocity increases with the increase of molecular additive, being the difference in the drift velocity larger as the drift electric field intensity decreases. This behavior is also demonstrated by Monte Carlo simulation results [51]. We note that typical drift electric field values in the NEXT TPC will be much lower than those used along this work, which are common for a scintillation region.

5. Conclusions

The most important conclusion that we can draw from this work is that, at least in the detector used, the Xe-CO_2 mixtures are not stable and, in addition, the getters do absorb CO_2 even at temperatures as low as 80ºC. These two facts are very serious drawbacks for considering CO_2 as a viable molecular additive to pure xenon in the NEXT TPC, in opposition to what simulations and our first experimental results would suggest. These results renovate, again, the importance of CH_4 as an alternative of molecular species as additive to pure xenon.

5.1. Future Work

As a future work a mass spectrometer should be used to have a reading of the true concentrations of CH_4 in the gas volume and to understand why Xe - CO_2 mixtures are not stable, even without the action of the getters. Measurements of the scintillation yield and energy resolution for Xe-0.2%CO_2 can be done, if stable enough conditions can be met within a period of time long enough to allow to perform such studies. Studies with Xe-CH_4 should have a higher priority; nevertheless, studies with Xe+0.5%CO_2 should be repeated to confirm the conclusions drawn from this work.

The experimental work with Xe-CH_4 mixtures could be repeated in NEXT-DEMO to measure electron transversal and longitudinal diffusion and electron drift velocity, as well as to measure the electron attachment probability and scintillation quenching for electron drift distances up to 30 cm, a must for fully understanding of the viability of such mixtures in NEXT-NEW.

Also, R&D, in the small detector in Coimbra should be implemented for Xe-CF_4 mixtures for CF_4 concentrations around or below 0.1% followed, if proved interesting enough, by similar studies in the NEXT-DEMO prototype.

References

[1] C.L.Cowan *et al*., Detection of the Free Neutrino: a Confirmation, Science 124 (1956) 103-104.

[2] B. T. Cleveland, T. Daily, J. Davis, Raymond, J. R. Distel, K. Lande, et al., Measurement of the solar electron neutrino flux with the Homestake chlorine detector, Astrophys. J. 496 (1998) 505-526.

[3] R. Wendell, C. Ishihara, K. Abe, et al., "Atmospheric neutrino oscillation analysis with subleading effects in Super-Kamiokande I, II, and III," Physical Review D, vol. 81, no. 9, Article ID 092004, 16 pages, 2010.

[4] B. Pontecorvo, "Inverse beta processes and nonconservation of lepton charge," Zhurnal Eksperimental'noi i Teoreticheskoi Fiziki, vol. 34, p. 247, 1957, Soviet Physics—JETP, vol.7, pp. 172-173, 1958.

[5] Ettore Majorana, Nuovo Cimento, 14 (1937) 171.

[6] M. Goeppert-Mayer, Double beta-disintegration, Phys.Rev. 48 (1935) 512.

[7] F.T. Avignone III et al., Double Beta Decay, Majorana Neutrinos, and Neutrino Mass, arxiv:0708.1033v2 [nucl-ex] (2007).

[8] S. R. Elliott, A. A. Hahn and M. K. Moe, Direct evidence for two-neutrino double beta decay in ^{82}Se, Phys. Rev. Lett. 59 (1987) 2020.

[9] A. Barabash, Review of double beta decay experiments, 2014, arXiv:1403.2870.

[10] Giulio Racah, Nuovo Cimento, 14 (1937) 322.

[11] W.H.Furry, Phys.Rev.56 (1939),1184.

[12] S.Davidson, E. Nardi, and Y. Nir, Leptogenesis, Phys. Rept. 466 (2008).

[13] J.J. Gomez-Cadenas et al. Letter of Intent: NEXT, a HPGXe TPC for neutrinoless double beta decay searches. (arXiv:0907.4054v1), April 2009.)

[14] H.V. Klapdor Kleingrothaus et al. Evidence for neutrinoless double beta decay. Mod. Phys. Lett. A, 16:2409-2420, 2001.

[15] SR. Elliot and P. Vogel., Annu. Rev. Nucl. Part. Sci., vol. 52, pp. 115–151,2002.

[16] W.C. Haxton et al. Radiochemical tests of double beta decay. Phys. Rev. C, 28:467-470, 1983.

[17] S. R. Elliott et al. Direct evidence for two-neutrino double-beta decay in ^{82}Se. Phys. Rev. Lett., 59:2020-2023, 1987.

[18] T. Kirsten. Geochemical double beta decay experiments. AIP. Conf. Proc., 66:396-410, 1983.

[19] O. K. Manuel. Geochemical measurements of double beta decay. J. Phys. G: Nucl. Part. Phys., 17:221-229, 1991.

[20] C.E. Aalseth, et al., Phys. Rev. D 70 (2004) 078302, http://arxiv.org/abs/nuclex/0404036v2.

[21] C. Arnaboldi, et al., Phys. Rev. C 78 (2008) 035502.

[22] HEIDELBERG-MOSCOW Collaboration, Phys. Rev. D 55 (1997) 54.

[23] C.E. Aalseth et al. Comment on evidence for neutrinoless double beta decay. Mod. Phys. A, 17:1475,2002.

[24] Y.G. Zdesenko et al. Has neutrinoless double beta decay of ^{76}Ge been really observed? Phys Lett. B, 546:206,2002.

[25] A. Barabash and the NEMO collaboration. NEMO 3 double beta decay experiment: Latest results. Journal of Physics: Conference Series, 173(1):012008, 2009.

[26] S. Schönert, et al., Phys. At. Nucl. 69 (2006) 2101.

[27] The Majorana Collaboration. White Paper on the Majorana Zero – Neutrino Double-Beta Decay Experiment. http://arxiv.org/abs/nucl-ex/0311013, 2003.

[28] M. Pedretti, et al., Int. J. Mod. Phys. A 23 (2008) 3395.

[29] A. Gando et al. Limits on majoron-emitting double-beta decays of ^{136}Xe in the KamLAND-Zen experiment. Phys. Rev. C, 86:021601R, 2012.

[30] R.S. Raghavan et al. New approach to the search for neutrinoless double beta decay. Phys. . Rev. Lett., 72:1411-1414, 1994.

[31] Akimov D. et al., EXO: An advanced Enriched Xenon double-beta decay Observatory, Nucl. Phys. Proc. Suppl. 138 (2005), 224.

[32] E. Aprile et al., New measurement of the relative scintillation efficiency of Xenon nuclear recoils below 10 keV, arXiv:0810.0274 [astro-ph].

[33] J. Angle et al., First Results from the XENON10 Dark Matter Experiment at the Gran Sasso National Laboratory, Phys. Rev. Lett. 100 (2008), 021303, arXiv: 0706.0039 [astro-ph].

[34] Elena Aprile, Laura Baudis, and for the XENON100 Collaboration, Status and Sensitivity Projections for the XENON100 Dark Matter Experiment, arXiv: 0902.4253 [astro-ph.IM].

[35] R. Luscher et al. Search for beta beta decay in Xe-136: New results from the Gotthard experiment. *Phys.Lett. B*, 434:407-414, 1998.

[36] Knoll GF. Radiation Detection and Measurement, (3rd edn). Wiley: New York, 2000.

[37] J.J. Gomez Cadenas, Private Communication, NEXT Colaboration.

[38] V. Alvarez et al. (NEXT Collaboration), NEXT-100 Technical Design Report (TDR), 2012 JINST 7 T06001.

[39] Physics and Engineering of Radiation Detection, by Syed Naeem Ahmed. ISBN-10 0-12-045581-1; ISBN-13 978-0-12-045581-2. Published by Academic Press, Elsevier, GB, 2007.

[40] Fano, U. (1947). "Ionization Yield of Radiations. II. The Fluctuations of the Number of Ions". Physical Review 72 (1): 26.

[41] Conde CAN, Policarpo AJPL. Nucl. Instrum. Methods 1967; 53: 7.

[42] A.J.P.L. Policarpo, M.A.F. Alves and C.A.N.Conde, The argon-nitrogen proportional scintillation counter, Nucl. Instrum. Meth., 55 (1967) 105) (C.A.N. Conde and A.J.P.L. Policarpo, A gas proportional scintillation counter, Nucl. Instrum. Meth., 53 (1967) 7-12.

[43] J. M. F. dos Santos, J. A. M. Lopes, J. F. C. A. Veloso, P. C. P. S. Simões, T. H. V. T. Dias, F. P. Santos, P. J. B. M. Rachinhas, L. F. Requicha Ferreira and C. A. N.

Conde, Development of portable gas proportional scintillation counters for X-ray spectrometry, X-Ray Spectrometry 30 (2001) 373-381.

[44] Freitas et. al, R&D Studies on the influence of the addition of percentage quantities of CH_4 to pure xenon, NEXT Internal Report, May 2014.

[45] P.C.P.S. Simões, D.S. Covita, J.F.C.A. Veloso et al., A new method for pulse analysis of driftless-gas proportional scintillation counters, Nuclear Instruments and Methods in Physics Research A 505:1-2 (2003) 247.4.

[46] SAES Getters, Via Gallarate, Milão, Itália; http://www.saesgetters.com.

[47] J. Escada, T.H.V.T. Dias, F.P. Santos et al, A Monte Carlo study of the fluctuations in Xe electroluminescence yield: pure Xe vs Xe doped with CH4 or CF4 and planar vs cylindrical geometries, JINST 6 (2011) P08006.

[48] C. M .B. Monteiro, L. M. P. Fernandes, J. A. M. Lopes, et al., Secondary scintillation yield in pure xenon, JINST 2 (2007) P05001.

[49] Y. Kondo, Y. Sekiya, M. Th. EL- Mohandes, Pulse Townsend Measurement of Electron Swarm Parameters at Low Pressure, International Journal of Emerging Technology and Advanced Engineering Volume 3 (2013) Issue 11.

[50] Jorge M.R., "Experimental measurement of the electroluminescence yield of pure xenon and mixtures of xenon with percentage quantities of CH4", Dissertação de Mestrado, Departamento de Física da Faculdade de Ciências e Tecnologia da Universidade de Coimbra, 2014.

[51] J. Escada, T.H.V.T. Dias, F.P. Santos et al., A Monte Carlo study of the fluctuations in xenon electroluminescence yield: pure xenon vs xenon doped with CH4 or CF4 and planar vs cylindrical geometries, JINST 6 (2011) P08006.